Suppression of epithelial proliferation and tumorigenesis by immunoglobulin A

Gregory P. Donaldson[1*], Gabriella L. Reis[1], Marwa Saad[1], Izabela Mamede [1], Guo Chen[1], Nicole L. DelGaudio[1], Dayu Zhang[2], Begüm Aydin[1], Caroline E. Harrer[1], Tiago BR Castro[1,3], Sergei Grivennikov[4], Bernardo S. Reis[1], Beth M. Stadtmueller[2,5,6], Gabriel D. Victora[3], and Daniel Mucida[1,7*]

[1]Laboratory of Mucosal Immunology, The Rockefeller University, New York, United States
[2]Department of Biochemistry, University of Illinois, Urbana, United States
[3]Laboratory of Lymphocyte Dynamics, The Rockefeller University, New York, United States
[4]Departments of Medicine and Biomedical Sciences, Cedars-Sinai Cancer, Cedars-Sinai Medical Center, Los Angeles, United States
[5]Carl R. Woese Institute for Genomic Biology, University of Illinois, Urbana, USA
[6]Department of Biomedical and Translational Sciences, Carle Illinois College of Medicine, University of Illinois, Urbana, USA
[7]Howard Hughes Medical Institute, The Rockefeller University, New York, United States

*Materials & Correspondence: gdonaldson@rockefeller.edu (G.P.D.) or mucida@rockefeller.edu (D.M.)

Abstract
Immunoglobulin A (IgA) is the most abundant antibody isotype produced across mammals and plays a specialized role in mucosal homeostasis[1]. Constantly secreted into the lumen of the intestine, IgA binds commensal microbiota to regulate their colonization and function[2,3], with unclear implications for health. IgA deficiency is common in humans but is difficult to study due to its complex etiology and comorbidities[4–8]. Using genetically and environmentally controlled mice, here we show that IgA-deficient animals have a baseline alteration in the colon epithelium that increases susceptibility to multiple models of colorectal cancer. Transcriptome, imaging, and flow cytometry-based analyses revealed that, in the absence of IgA, colonic epithelial cells induce antibacterial factors and accelerate cell cycling in response to the microbiota. Oral treatment with IgA was sufficient to suppress aberrant epithelial proliferation independently of bacterial binding, suggesting that IgA provides a feedback signal to epithelial cells in parallel with its known roles in microbiome shaping. In a primary colonic organoid culture system, IgA directly suppresses epithelial growth. Conversely, the susceptibility of IgA-deficient mice to colorectal cancer was reversed by Notch inhibition to suppress the absorptive colonocyte developmental program, or by inhibition of the cytokine MIF, the receptor for which was upregulated in stem cells of IgA-deficient animals. These studies demonstrate a homeostatic function for IgA in tempering physiological epithelial responses to microbiota to maintain mucosal health.

Main

In the absence of infection or disease, IgA is constantly produced in the intestine, where it is secreted into the lumen in the form of secretory IgA and binds commensal microbiota[9]. In humans, selective IgA deficiency is the most common primary immunodeficiency, clinically defined as having low (<7 mg/dL) serum IgA levels with normal levels of IgM and IgG[10]. These patients have an increased risk of respiratory/gastrointestinal infections, inflammatory/autoimmune disorders[10], and gastrointestinal cancers[11]. IgA is known to control mucosal pathogens[12–14], but the impact of IgA on inflammatory diseases and malignancy remains unclear. Recent studies have indicated that IgA deficiency is associated with changes in microbiota and systemic inflammation[4,6,7,15], which may be more pronounced in patients with undetectable IgA[8]. A compensatory increase in the other major secreted antibody isotype, IgM, is insufficient to rescue these effects[4]. The association with malignancy, first observed clinically decades ago[16,17] may be related to the impact of gut microbiota on colon cancer[18–20]. The largest study on IgA deficiency (2,495 patients matched to 24,509 controls) showed doubled all-cause mortality and an increased risk of colon and prostate cancers[21]. An inverse analysis of patients with gastrointestinal cancer found increased frequency of IgA deficiency[22]. Among patients with combined variable immunodeficiency, those with colon cancer were more likely to have a deficiency in IgA[23]. Despite these associations, the polygenic nature of IgA deficiency, clinical criteria based on an arbitrary cutoff for serum (not mucosal) concentration, and various comorbidities thwart the attribution of these health effects to isotype-specific functions.

Most of the known functions of intestinal IgA have been discovered using mouse models, showing that these antibodies prevent mucosal infections[12–14] and affect the form and function of the gut microbiome[24–31]. IgA can be polyreactive[32,33], cross-reactive[34,35], or species-specific[36], allowing binding to a substantial fraction of the mammalian microbiota at the cellular level. Effects on bacteria can vary; IgA controls *Bacteroides thetaiotaomicron* gene expression[37,38], *Salmonella enterica* swimming motility[14], *Bacteroides fragilis* mucosal anchoring[39], and *Escherichia coli* surface receptor activities[40]. But beyond limiting invasive pathogenesis, mechanisms connecting microbiota-IgA interactions to health and disease are lacking. An isotype-specific knockout mouse model (*Igha*$^{-/-}$ hereafter referred to as IgA$^{-/-}$) causing total IgA deficiency was made more than 20 years ago[41]. This causes an increase in serum and mucosal IgM levels[41], which is often observed in human IgA deficiency[4]. IgA$^{-/-}$ mice have a few described phenotypes[13], and are largely indistinguishable from wild-type controls in a dextran sodium sulfate colitis model[42], suggesting that IgA is dispensable for normal intestinal barrier. In contrast, polymeric immunoglobulin receptor (PIgR) knockouts, which are unable to actively transport antibodies to the lumen of the intestines, are more susceptible to colitis[42], highlighting the importance of compensatory IgM or other functions of PIgR in supporting the barrier. PIgR binds dimeric IgA or pentameric IgM and directs their transcytosis and secretion into the gut lumen. The cleaved ectodomain of PIgR remains attached to the antibody, known as the secretory component, which can bind bacteria independent of antibody[43,44]. While many secreted host factors interact with bacteria to reinforce the epithelial barrier, IgA may have more nuanced roles, which may explain the perplexing epidemiology of human IgA deficiency.

Impact of IgA deficiency during steady state and cancer models

To study the direct physiological consequences of IgA deficiency and the fundamental isotype-specific functions of IgA in the gut, female IgA$^{+/-}$ mice were bred with IgA$^{-/-}$ males to control for effects of maternal milk IgA on normal immune development[45]. IgA$^{+/-}$ mice had comparable levels of fecal IgA to IgA$^{+/+}$ littermates (**Extended Data Fig. 1a-b**), indicating that heterozygotes can serve as a normal control. Co-housed littermates were used in all experiments to minimize environmental variables and normalize the microbiome through both vertical and horizontal transmission[46]. For an unbiased analysis of possible IgA effects on the region of the gut with the highest concentration of gut bacteria[47], mid-colon tissues were sampled at steady state for bulk RNA-Seq (**Fig. 1a**). Overall, the number of differentially expressed genes was modest, and there was no evidence of overt inflammation in the IgA$^{-/-}$ colon. Nevertheless, IgA$^{-/-}$ mice showed alterations in many epithelial-related genes, including a decrease in goblet cell markers (*Spink4*, *Fcgbp*, *Capn9* and *Tff3*) and other cell type-specific markers such as *SpiB* (M cell transcription factor) and *Rgs4* (enteroendocrine cell marker) (**Fig. 1a, Supplementary Table 1**). This coincided with an increase in *Nox1*, a specific marker for the highly proliferative transit-amplifying cells[48], with concordant increases in general cell cycling-related pathways and

specific genes (*Mcc* and *Sass6*) (**Fig. 1a**). These results point to a physiological role for IgA in balancing proliferation and differentiation in the intestinal epithelium.

Next, we used a murine model of endogenous colon cancer as a perturbation to test for further effects of IgA revealed by the disease state. IgA$^{-/-}$ mice were crossed to a strain harboring a *Cdx2* promoter-driven, tamoxifen-inducible Cre recombinase and loxP-flanked alleles of the tumor suppressor *APC*, which is mutated in more than 90% of human colorectal tumors[49,50]. This allows for temporally controlled homozygous knockout of *APC* in a fraction of colon epithelial cells (**Fig. 1b**). To compare to the steady-state transcriptome changes observed in IgA$^{-/-}$ colon samples, we harvested tissue for the same analysis at an early, pre-tumor time point (**Fig. 1b-c**). Despite the synchronized loss of APC in these co-housed littermates, there were substantial (hundreds of genes) and complex differences in gene expression patterns between IgA$^{+/-}$ and IgA$^{-/-}$ animals (**Extended Data Fig. 1c, Supplementary Table 2**). Specifically, pathways related to epithelial proliferation, APC mutation, and human colorectal cancer were enhanced in IgA$^{-/-}$ mice (**Fig. 1c**). At the pathway level, modest alterations at steady state in IgA$^{-/-}$ mice mirrored the more dramatic phenotype induced by APC mutation (**Fig. 1c**). Analysis of the specific genes altered during steady state showed that a majority of these IgA modulated genes were also modulated by *APC* loss, with nearly perfect directional concordance between IgA deficiency and *APC* loss (**Extended Data Fig. 1d**). These molecular results were predictive of gross morphological outcomes (**Fig. 1d**). While IgA$^{+/+}$ and IgA$^{+/-}$ mice were indistinguishable (**Extended Data Fig. 1e**), IgA$^{-/-}$ mice had shortened colons (**Fig. 1e**), increased number of tumors (**Fig. 1f**) and increased total tumor load (**Fig. 1g**) when compared to cohoused IgA$^{+/-}$ littermates. The size of tumors was similar between genotypes (**Fig. 1h**). Though this model is dependent on inflammation-driven tumor growth[49,50], fecal lipocalin as a measure of inflammation (**Extended Data Fig. 1f**), and expression levels of cytokines in the bulk RNA-Seq (**Extended Data Fig. 1g**) showed no differences in IgA$^{-/-}$ mice, suggesting that the impact of IgA was not related to general increases in inflammatory signals. These molecular and tumor analyses indicate that IgA$^{-/-}$ mice are more susceptible to a model of endogenous colorectal cancer. This effect may be due to alterations in the steady state that promote tumorigenesis.

To expand on these findings, IgA$^{+/-}$ and IgA$^{-/-}$ mice were subjected to an independent colorectal cancer model in which injection of the mutagen azoxymethane is followed by three rounds of exposure to dextran sodium sulfate (AOM-DSS) in their drinking water (**Fig. 1i**). This mimics colitis-associated cancer, which accounts for approximately 5% of human colorectal cancer patients[50]. IgA$^{-/-}$ mice had similar colon length (**Fig. 1j**) but showed more tumors (**Fig. 1k**), and higher overall tumor load (**Fig. 1l**) than IgA$^{+/-}$ controls. As previously reported, IgA$^{-/-}$ mice were slightly more susceptible to DSS-induced weight loss (**Extended Data Fig. 1h**). Whereas most IgA$^{-/-}$ mice developed tumors even when exposed to a relatively low dose of DSS (1.5%), a minority of IgA$^{+/-}$ mice developed tumors (**Extended Data Fig. 1i**). The average tumor size was comparable among the tumor-bearing animals, (**Fig. 1m**). These results are consistent with the APC-driven model, suggesting a specific role for IgA in tumorigenesis but not growth. To directly test whether IgA affects tumor growth, IgA$^{+/-}$ and IgA$^{-/-}$ mice were subjected to a model that bypasses the transformation stage. Mouse colon organoids with four cancer-related gene mutations (*APC*, *KRas*, *P53*, *Smad4*) were dissociated into single cells, injected by colonoscope directly into the colon wall and monitored every two weeks by colonoscopy (**Fig. 1n**). These implanted tumors grew at a similar rate (**Fig. 1o**), with a similar frequency (**Fig. 1p**), and were similar in size at the endpoint (**Fig. 1q**). Overall, our data indicate that IgA has no apparent role in controlling tumor progression but actively regulates early tumorigenesis in the colon.

The role of IgA-bacteria interactions on tumor susceptibility

As the primary known function of IgA at steady state is to regulate the composition and function of microbiota, we investigated whether IgA$^{-/-}$ mice harbor a pro-tumor microbiome despite being cohoused with littermates. The role of bacteria was first assessed by treating mice with a cocktail of broad-spectrum antibiotics (ampicillin, vancomycin, metronidazole, neomycin, or AVNM) throughout the experiment (**Fig. 2a**). AVNM treatment reduced tumor numbers in all mice, as previously reported in this model[49], but also prevented the heightened tumor phenotype observed in untreated IgA$^{-/-}$ mice (**Fig. 2b**). To profile the bacterial microbiome and identify IgA-dependent changes that might explain the observations in Fig. 1, 16S rRNA amplicon sequencing was

performed in healthy mice at steady state and two weeks after *APC* deletion. IgA$^{-/-}$ mice were indistinguishable from littermate controls when inheriting an identical starting microbiome and were co-housed throughout the experiment (**Fig. 2c, Extended Data Fig. 2a**). *APC* loss caused a shift in the microbiome, with a loss of diversity including the depletion of species within the common mouse commensal family *Muribaculaceae* (**Fig. 2c**). This coincided with the outgrowth of *Shigella* and *Helicobacter* species (**Fig. 2c**), both of which have been implicated in colorectal cancer[18–20]. During this dramatic change, IgA still had no apparent influence, at least in the cohoused conditions of these experiments (**Fig. 2c, Extended Data Fig. 2a**). As some IgA-mediated alterations have previously been shown to be mucus-specific[26,39], the colon mucus was sampled aseptically for microbiome profiling. This analysis successfully resolved the spatial differences in lumen and mucosal community compositions (**Extended Data Fig. 2a-b**)[47], and revealed that some commensal mucosal species of *Akkermansia* and *Bacteroides* were resilient to *APC* loss (**Extended Data Fig. 2b**). However, even in mucus, no differences were apparent between IgA$^{+/-}$ and IgA$^{-/-}$ samples (**Extended Data Fig. 2a-b**). A statistical test for differential abundance of amplicon sequence variants in microbial communities (ANCOM)[51] revealed no differences between IgA genotypes in colon lumen or mucus, at steady state, or in the context of *APC* loss (**Extended Data Fig. 2c**). The fact that these mice developed more tumors (*see* Fig. 1) despite the lack of an IgA-dependent microbiome signature was initially counterintuitive. These results indicate that IgA may suppress tumor initiation in a manner that depends on the presence of bacteria but is independent of microbiome shaping.

To dissect the potential alternative mechanisms by which IgA prevents tumorigenesis, sufficiency experiments were performed to rescue the defects in IgA$^{-/-}$ mice (**Fig. 2d**). First, sterile-filtered fecal extracts (containing proteins and soluble metabolites, **Fig. 2e**) from healthy mice were used for a daily oral gavage starting prior to the induction of *APC* loss. Although treatment was ceased 3 weeks prior to measuring tumors, extracts from IgA$^{+/-}$ but not IgA$^{-/-}$ mice were sufficient to reduce tumor load in the IgA$^{-/-}$ recipients (**Fig. 2f**). To test whether this impact is conferred by the antibodies or other components of the extract, secretory IgA was purified from feces of healthy mice (**Fig. 2e**) and gavaged daily in the same timeframe. This polyclonal IgA preparation from healthy mouse feces was also sufficient to protect IgA$^{-/-}$ mice from increased tumors (**Fig. 2g**). The IgA oral treatment model allowed for the manipulation of antigen specificity, first by purifying IgA from the feces of germ-free Swiss Webster mice mono-colonized with the model commensal species *Bacteroides fragilis*. Despite the restricted mucosal antigen exposure under these conditions, IgA purified from these mice was also sufficient to protect IgA$^{-/-}$ mice from increased tumor load (**Fig. 2h**). Additionally, analyses of recipient feces during this treatment revealed no coating of the microbiota (**Extended Data Fig. 3a**), raising the possibility that the impact on tumorigenesis is independent of bacterial binding. Consistent with this, recombinant monoclonal secretory IgA specific for influenza HA (CR9114) protected IgA$^{-/-}$ mice from increased tumor formation (**Fig. 2i**). This effect was not mediated by the secretory component alone and instead required the full structure of secretory IgA (**Fig. 2j**). This indicates that antibody specificity is irrelevant to the IgA-mediated suppression of tumor initiation in the colon. In all cases, oral treatments that reduced tumor load did not affect the average size of tumors (**Extended Data Fig. 3b-e**). Coupled with a lack of alterations to the microbiota, these results suggest that IgA may directly alter epithelial cells to influence the chances of tumor initiation or outgrowth.

Impact of IgA on epithelial cells

To further investigate how IgA may impact the steady-state epithelium, mid-colon epithelial cells were sorted (live CD45- EPCAM+, **Extended Data Fig. 4a**) for single-cell transcriptomics from three IgA$^{+/-}$ mice and three IgA$^{-/-}$ littermates (**Fig. 3a-b**). Clusters were identified based on known markers, such as stem (*Lgr5*+) and transit-amplifying (*Mki67*) cells partially overlapping in clusters 0, 5, and 9, and goblet cells in clusters 6, 8, and 10 expressing the secretory progenitor marker *Atoh1* (Fig. 1a, c, **Extended Data Fig. 4b**). In terms of cellular composition, IgA$^{-/-}$ mice had slightly more *Reg3b*-expressing colonocytes in cluster 1 and slightly fewer absorptive *Aqp8*+ colonocytes in cluster 2 (**Fig. 3c-d**). However, the clearest difference in cellularity was the increased number of proliferating or immature colonocyte progenitors in IgA$^{-/-}$ mice (cluster 5, **Fig. 3d**). Cluster 5 was distinctly marked by *Hao2* expression (Fig. 1c), cell cycling (*Mki67*, Fig. 1c), and expression of the canonical Notch target, *Hes1* (**Extended Data Fig. 4c**), which further identifies them as progenitors of the absorptive lineage[52]. The lack of *Muc2* expression is also evidence of their undifferentiated state (**Extended**

Data Fig. 4b). The expansion of these cells in IgA$^{-/-}$ mice suggests an alteration in the development of colonic epithelial cells.

In terms of gene expression, when analyzing all cells together, IgA deficiency resulted in only a handful of differentially expressed genes (**Supplementary Table 3**). Several genes encoding secreted antimicrobial peptides, such as *Dmbt1*, *Reg3b*, and *Reg3g*, were highly expressed in colon epithelial cells from IgA$^{-/-}$ mice (**Fig. 3e**). These specific genes were previously found to be induced at the single-cell level by bacterial colonization of germ-free mice[53]. At the pathway level, epithelial cells from IgA$^{-/-}$ mice showed a decrease in interferon signaling and an increase in antimicrobial responses but not a general inflammatory response (**Fig. 3f**). Pathways related to proliferation and central metabolism were up in IgA$^{-/-}$ mice, while adhesion and tight junction pathways had cell type-specific changes (**Fig. 3f**). The highly proliferative cluster 9 exhibited enrichment of the pre-notch reactome in IgA$^{-/-}$ mice (**Fig. 3f**), which may steer the cycling cells toward the absorptive fate and cluster 5. Collectively, analysis of the colon epithelial transcriptome at the single-cell level in IgA-/- mice revealed alterations in the local response to microbiota, as well as changes in epithelial development related to proliferating populations.

IgA suppresses tumorigenesis by restricting epithelial proliferation

To directly assess the effects of IgA on epithelial proliferation, we measured incorporation of 5-ethynyl-2-deoxyuridine (EdU) into the DNA of dividing cells. Mice were injected 24 h and 4 h before tissue harvest to label all cells proliferating within one day. Using a counterstain of EPCAM (green) to visualize crypt structures, EdU+ cells (pink) were quantified in frozen sections (**Fig. 4a**). IgA$^{-/-}$ mice showed increased numbers of EdU+ cells per crypt (**Fig. 4b**), which was consistent with an increased rate of epithelial proliferation. As colon epithelial cycling was previously shown to be a physiological response to microbial stimulation through TLR signaling[54], IgA$^{-/-}$ mice were rederived germ-free to test whether the enhanced epithelial proliferation was dependent on the microbiota. In these animals, quantification of EdU+ cells in frozen sections showed no difference (**Extended Data Fig. 5a**). To confirm the change in proliferation, we used an orthogonal method of intracellular Ki67 staining by flow cytometry of isolated colon epithelial cells (**Fig. 4c, Extended Data Fig. 5b**). Consistent with the EdU results, colon epithelial cells from IgA$^{-/-}$ mice were more frequently Ki67+ (**Fig. 4d**). Gavaging IgA$^{-/-}$ mice with monoclonal anti-influenza SIgA was sufficient to reduce Ki67 staining to the level of IgA$^{+/-}$ littermate controls (**Extended Data Fig. 5c**). To test whether IgA can directly interact with epithelial cells to alter their proliferation, an *in vitro* entero-organoid culture system starting with primary isolated colon crypts was used to mimic normal epithelial developmental processes. Despite the lack of microbial stimulation in culture, high Wnt media and Matrigel optimized to support entero-organoid cultures provide many growth-enhancing signals[55,56]. Colonic crypts isolated from IgA$^{-/-}$ mice were cultured as 3-dimensional organoids and subsequent treatment with SIgA, but not IgG, reduced the number of organoids recovered (**Fig. 4e-f**). Coupled with the irrelevance of antigen specificity to this IgA function, this indicates that IgA suppresses epithelial proliferation via a direct interaction. Although independent of bacterial binding, this effect of IgA is reciprocal to the physiological epithelial stimulation provided by microbiota[54].

The developmental pathway leading to absorptive colonocyte precursor proliferation, to the exclusion of secretory cell fate, appears to be enhanced in the colon epithelium of IgA$^{-/-}$ mice (Fig. 3). As this pathway is dependent on Notch signaling[57], treatment with the Notch inhibitor dibenzazepine inhibits proliferation and forces epithelial stem cell differentiation towards goblet cell fate[58]. A low-dose treatment regimen beginning prior to the induction of APC loss did not affect the tumor outcome in IgA$^{+/-}$ mice but prevented the increased tumor burden previously observed in IgA$^{-/-}$ mice (**Fig. 4g-h**). In the context of IgA deficiency and in this cancer model, Notch inhibition phenocopies the effect of oral treatment with IgA, supporting the notion that IgA$^{-/-}$ mice develop more colonic tumors because of accelerated or dysregulated epithelial proliferation. Indeed, the single-cell transcriptome revealed alterations upstream of Notch that could plausibly cause enhanced proliferation. Within cluster 0, which contains stem cells expressing *Lgr5* (Fig. 3a,c), cells isolated from IgA$^{-/-}$ mice showed increased expression of a subset of MHC class II genes (**Extended Data Fig. 4d**). Overall, MHCII expression in epithelial cells was previously associated with proliferation in response to microbiota[59,60]. Amongst these genes, the most highly expressed and most highly upregulated in IgA$^{-/-}$ mice was the MHCII

invariant gamma chain, *CD74* (**Fig. 4i, Extended Data Fig. 4d-e**). When expressed in excess, a portion of CD74 is trafficked to the cell membrane where it functions as a receptor for the cytokine MIF, which induces cell cycling[61]. Downstream intracellular signaling requires co-expression of CD44, which binds CD74 as a heterodimer[62]. The colon stem cells in cluster 0 not only expressed *CD74* and *CD44* but also *Mif*, allowing for autocrine signaling to drive epithelial proliferation (**Extended Data Fig. 4e**). Supporting a pro-cancer role for MIF signaling, *CD74*, *CD44*, and *MIF* are upregulated in human colorectal tumor cells compared to normal colon epithelia[63].

Several methods have been used to address the contribution of MIF signaling to IgA-related phenotypes observed. First, to determine whether surface MIF receptor is modulated by IgA, colon epithelial cells were isolated and analyzed by flow cytometry. $IgA^{-/-}$ mice showed a higher frequency of cells with both CD44 and CD74 on their surface (**Fig. 4j-k**). MIF signaling via CD74/CD44 leads to ERK activation in epithelial cells, which induces proliferation[64]. To assess the involvement of this pathway, colonic epithelial cells were isolated and lysed for analysis by ELISA. Colon epithelial cells from $IgA^{-/-}$ mice had a higher proportion of phosphorylated ERK than cells from control mice (**Fig. 4l**), consistent with enhanced MIF signaling. To determine whether MIF signaling contributes to the effects of IgA on epithelial proliferation *in vivo*, mice were treated with a selective inhibitor, 4-iodo-6-phenylpyrimidine (4-IPP), which irreversibly binds MIF and prevents interaction with CD74[65]. Treatment for ten days normalized Ki67 staining of colon epithelial cells in $IgA^{-/-}$ mice (**Extended Data Fig. 5d**), linking aberrant proliferation to MIF signaling. Accordingly, 4-IPP treatment prior to induced APC loss resulted in indistinguishable tumor burden phenotypes in $IgA^{-/-}$ and $IgA^{+/-}$ littermate control mice (**Fig. 4m-n**). These data show that enhanced MIF signaling via the IgA-modulated receptor CD74 in epithelial stem cells is associated with accelerated epithelial cycling and increased susceptibility to colorectal cancer in $IgA^{-/-}$ mice.

Discussion

Through its effects on epithelial cells, IgA in the lumen of the gut lowered the risk of colon tumor initiation in mouse models. Although IgA was previously reported to suppress growth of ovarian tumors through interactions with immune cells and PIgR, which is highly expressed in ovarian tumors[66], we did not observe an impact of IgA on tumor growth in the colon. *PIGR* is also dramatically downregulated in human colorectal tumors[63]. Fecal IgA levels have been reported to be elevated in colorectal cancer patients[67], though the functional roles for IgA in colorectal cancer have not been previously addressed. Interventions that can prevent tumor emergence in gastrointestinal cancers are lacking beyond general guidance regarding healthy diet and lifestyle. Unlike other body sites, there is substantial evidence for a bacterial role in tumor initiation in the colon[68]. The development of preventative measures to reduce the incidence of colorectal cancer requires a deeper study of the physiological mechanisms that maintain homeostasis at the epithelial border flanked by gut microbiota.

This study establishes a new role for IgA in suppressing epithelial proliferation. In our murine models, IgA appears to suppress the dynamic responses of colonic epithelial cells to microbiota. These findings are consistent with early microarray experiments of small intestinal samples from B cell-deficient and $IgA^{-/-}$ mice, which detected increased expression of genes encoding antimicrobial peptides[24]. Authors also observed that induction of compensatory IgM in the $IgA^{-/-}$ animals had a minimal impact on gene expression changes[24]. Similar conclusions have been drawn in *Pigr*$^{-/-}$ mice[69]. While the role of IgA in shaping microbiota form and function is well established, here we found a parallel, homeostatic function of IgA in the colon lumen, akin to cytokine-like signaling. If microbial stimulation of epithelial cells provides an "accelerate" signal for proliferation and antimicrobial function, IgA stimulation appears to be a "brake" to modulate these behaviors. How epithelial cells sense this signal remains unknown. PIgR is localized to the basolateral side of epithelial cells and moreover cannot bind secretory IgA, making it unlikely to be involved in IgA feedback signaling to the epithelium. In secretory IgA, the Fc portion of the antibody is partially obscured by the SC[70], and colon epithelial cells do not express a typical Fc receptor that binds the alpha heavy chain. However, many proteins have reported interactions with IgA, leaving open the possibility of a non-conventional antibody receptor being responsible for such epithelial feedback.

The incredible quantity of IgA secreted into the lumen at steady state is sufficient to support its multiple functions. Despite coating a substantial fraction of the microbiota at the cellular level, IgA remains in excess at the luminal surface. It is estimated that approximately 95% of IgA in the intestinal lumen is unbound[71] and is, therefore, presumably available for epithelial feedback. Whether similar impacts of IgA occur in humans remains to be defined and will require dedicated studies. If so, alterations in the epithelial responses to microbiota may be a primary consequence of total mucosal IgA deficiency, a human condition that remains mysterious and difficult to study. The impact of IgA on epithelia as well as microbiota may intersect with genetic and environmental factors to manifest in patient-specific outcomes[4,7,10,11,72].

Author contributions
G.P.D. and D.M. conceived and initiated the project. G.P.D. designed and performed most of the experiments, with guidance from D.M. G.L.R. performed organoid experiments, purified IgA, and assisted most of the experiments. M.S. performed colonoscopy procedures. G.P.D. analyzed 16S rRNA amplicon sequencing, I.M. analyzed single-cell RNA-Seq, and G.C. analyzed bulk RNA-Seq, with guidance from T.B.R.C. N.L.D. performed flow cytometry experiments and C.H. performed fluorescence imaging. D.Z. and B.M.S. designed and produced recombinant secretory component and IgA variants. G.P.D., B.A., and B.S.R designed and executed epithelial cell sorting and single-cell RNA-Seq. S.G., B.S., B.S.R, G.D.V., and D.M. provided guidance and assisted in experimental design and interpretation. G.P.D. and D.M. wrote the manuscript and all authors edited the manuscript.

Acknowledgements
The authors thank Sohail Tavazoie (Rockefeller), Jeremiah Faith (Mt. Sinai), Duane Wesemann (Brigham and Women's), Meghan Koch (Fred Hutchinson), and members of the Mucida and Victora labs at Rockefeller for useful discussions. Germ-free mice were generated and maintained by Aneta Rogoz at Rockefeller University. Animals were monitored and cared for by the staff of the Comparative Bioscience Center at Rockefeller University. Sequencing was performed by the Rockefeller University Genomics Core. Sarah Leonard assisted with protein purifications at University of Illinois. G.P.D. was a Robert Black Fellow of the Damon Runyon Cancer Research Foundation (DRG-2362-19). G.L.R. was supported by a scholarship from Fundaçao Maria Emília (Brazil). Project initiation was supported by pilot grants from the Rockefeller University Center for Basic and Translational Research on Disorders of the Digestive System through the generosity of the Leona M. and Harry B. Helmsley Charitable Trust and the Shapiro-Silverberg Fund for the Advancement of Translational Research to G.P.D. The project was further funded by grants from the NIH to B.M.S. (R01AI165570), from the NIH to G.D.V. and D.M. (R01AI157137) and from HHMI to D.M.

Competing interests
The authors declare no competing interests.

Methods
Mice
All mice were housed at the Rockefeller University and handled in accordance with protocols approved by the Institutional Animal Care and Use Committee (IACUC) and under the ethical guidelines within in the National Institutes of Health (NIH) Guide for the Care and Use of Laboratory Animals. C57BL/6J (000664) and *Cdx2*^{CreER} (022390) mice were purchased from Jackson Laboratories. *IgA*$^{-/-}$ mice on a C57BL/6J background were provided by Margaret Conner (Baylor) and *APC*$^{fl/fl}$ mice on a C57BL/6J background were provided by Sergei Grivennikov (Cedars-Sinai). These mice were housed in Specific Pathogen Free conditions on a fixed 12 hour light-dark cycle with food and water provided *ad libitum*. *IgA*$^{+/-}$ mice were rederived by c-section into germfree flexible film isolators (Class Biologically Clean) that were routinely monitored by quantitative real time PCR. Germfree mice were housed with a fixed 12 hour light-dark cycle with autoclaved food and water provided *ad libitum*. The genotype of mice was determined by quantitative real time PCR analyses by Transnetyx. The IgA genotype of mice was routinely cross-checked using ELISA or flow cytometry. For experiments comparing *IgA*$^{+/-}$ to *IgA*$^{-/-}$, littermate, sex-matched controls were co-housed from weaning through the duration. During data collection, mice were identified only by an experiment name and ear punch, which was matched to genotype post hoc. Experiments were initiated when mice were aged 8-10 weeks, unless otherwise noted. Both male and female mice were used for all experiments, analyzed separately, and then pooled if no sex differences emerged. Estrous cycle was not controlled for.

Murine cancer models
For all cancer models, animals were monitored daily for sickness behavior and weighed at least twice per week to assess health and maintain a humane endpoint if weight loss exceeded 20% of their initial weight. For the APC model, *Cdx2*^{CreER}*APC*$^{fl/fl}$ mice were injected intraperitoneally at day 0 and day 3 with 0.8 mg tamoxifen (Sigma) from a stock solution at 4 mg/ml dissolved in corn oil (Sigma). After 4 weeks (day 28), mice were

sacrificed to count and measure tumors. For the AOM-DSS model, mice were injected intraperitoneally with 12.5 mg/kg azoxymethane (AOM) at day 0. Exposure to 1.5% dextran sodium sulfate (DSS) in drinking water replaced their normal water for 1 week starting at day 0. This was followed by a 2 week break, a second DSS exposure for 1 week, a 2 week break, and a third exposure for 1 week. Animals were sacrificed at day 100 to measure and count tumors. Lipocalin-2 was measured using the Mouse Lipocalin-2/NGAL DuoSet ELISA kit from R&D Systems (Cat. DY1857) according to manufacturer's protocol. For the pre-cancerous organoid implant model, $IgA^{+/-}$ and $IgA^{-/-}$ mice were injected with 1.5 $x10^5$ cells of quadruple-knockout AKPS organoids (*APC*, *Kras*, *P53*, *Smad4*; generated in Sergei Grivennikov's laboratory). Cells were injected over 3 injections (5 $x10^4$ cells in 40 uL each), spaced ~ 0.5 cm apart in the distal colon and rectum wall using a colonoscope (Karl Storz, Model TC300) with a custom-made 33-gauge needle (Hamilton Company). AKPS organoids were cultured by resuspending organoid cells in 50% matrigel (Corning) in cold ADF^+ media (Advanced DMEM F12 (Invitrogen) supplemented with 5% heat inactivated FBS (Sigma-Aldrich), 1% Penicillin-Streptomycin-Glutamine (Invitrogen), 1% HEPES (Invitrogen)). In a 6-well plate, 40 uL droplets of cell suspension were plated and incubated at 37°C for 20 minutes, followed by adding 3 mL of pre-warmed ADF^+ media. To prepare cells for injections, AKPS organoids were dissociated with cold ADF^+ media to break down matrigel, and spun down at 350g for 5 minutes. Organoid pellet was resuspended in Tryple Express Enzyme (Thermo Fisher Scientific) and incubated at 37°C for 30 minutes with shaking at 120 rpm. Organoids were further broken down into cells by pipetting multiple times with P1000, followed by washing with ADF^+ media and spinning down at 350g for 5 minutes. Cells were resuspended in ADF^+ media for counting, then volume was further adjusted to keep cells at 1250 cells/uL in 10% matrigel, 1% filter-sterilized Methylene Blue (Biopharm, Amazon), and 10 uM Y27632 (Stemcell Technologies). Implanted tumors were monitored every two weeks using the colonoscope and were scored according to previously used criteria (1: small but detectable tumor, 2: tumor covering one-eighth of colon circumference, 3: tumor covering one-fourth of colon circumference, 4: tumor covering one-half of colon circumference)[73].

Interventions in APC cancer model

For antibiotic depletion of the microbiome, mice were provided with sterile-filtered drinking water with 1 mg/ml ampicillin, 1 mg/ml neomycin, 0.5 mg/ml vancomycin, and 0.5 mg/ml metronidazole, supplemented with 10 mg/ml sucralose for palatability. For oral gavage treatments to rescue IgA deficiency, mice were subjected to a daily intra-gastric gavage with 2.5 µg of IgA (or the equivalent) in 200 µl PBS. For Notch inhibition, mice were given a daily 3 µmol/kg intraperitoneal injection of dibenzazepine (DBZ) (StemCell Technologies) which was first dissolved as a 10 µmol/ml in DMSO stock solution (kept frozen at -20C) and then diluted in 0.5% hydroxypropyl methylcellulose for injection. For inhibition of MIF cytokine signaling, the selective MIF inhibitor, 4-iodo-6-phenylpyrimidine (4-IPP) (Calbiochem CAS 41270) was injected intraperitoneally at 5 mg/kg every 48 hours.

Bulk RNA-Seq

Working on ice with one animal at a time until samples were homogenized by bead beating to stabilize RNA, mice were sacrificed by cervical dislocation, the colon was dissected, cut open longitudinally, and washed 3 times in PBS to remove lumen contents. An approximately 0.5 cm x 0.5 cm sample of tissue from the mid-colon (3 cm distal from the cecal junction) was collected in a Lysing Matrix D tube (MP Biomedicals) with 1 ml Trizol (Invitrogen) and beat at max speed for 60 seconds (MP Biomedicals FastPrep 24 Bead Beater), twice, with 5 minutes rest on ice between. Total RNA was purified according to the manufacturer's instructions for Trizol, followed by further purification using a Qiagen RNeasy column with on-column DNase treatment (Qiagen) according to the manufacturer's instructions. RNA quality was assessed using an Agilent Bioanalyzer and only samples with RIN > 8.0 were used for poly-A selected mRNA-Seq. Libraries were sequenced on an Illumina NextSeq 500 high-throughput flow cell, with a single-end 75 bp read, yielding between 23 and 30 million high quality paired-end reads per sample. STAR aligner 2.7.10a and biomaRt 2.52.0 were used to align reads and annotate genes with the GRCm39 mouse genome and M32 mouse transcriptome. Differential expression analyses was performed using DESEq2 1.36.0 and gene set enrichment analyses using fgsea 1.22.0 with gene sets c2.cgp.v7.5.1.symbols and c5.go.bp.v7.5.1.symbols.

16S rRNA amplicon sequencing

Mice were sacrificed by cervical dislocation and the colon was dissected and opened longitudinally on ice using autoclaved tools and aseptic technique. Lumen samples were taken from the mid colon, then the tissue was washed thoroughly 3 times in sterile PBS on ice, dabbed several times on a sterile petri dish to dry, and mucus was gently scraped from the tissue using a plastic cell scraper. All samples were frozen and -80C prior to further processing. DNA extraction was performed using the QIAamp PowerFecal Pro DNA Kit (Qiagen) with bead beating on an MP Biomedicals Fastprep 24, according to manufacturer's protocols. To avoid contaminating the lower biomass samples, mucus samples were processed separately, with decontamination of benches, racks, pipettes, and microcentrifuge prior to processing. 16S rRNA was amplified and libraries were prepared and pooled according to the Earth Microbiome Project 16S Illumina Amplicon protocol (earthmicrobiomeproject.org). Sequencing was performed with an Illumina MiSeq 150 bp paired-end run. The data were analyzed using the Qiime 2 (v2022.8) package. Amplicon sequence variants (ASVs) were identified and chimeric sequences were removed using Deblur. Phylogenetic analyses were performed using the Qiime 2 classifier trained on the SILVA database (v138) from 515F to 806R to match the amplicon sequencing. Following the Deblur processing, only samples with more than 1000 reads were included and only features with at least 100 reads across all samples that were present in at least 5 different samples were included.

Fecal IgA purification

IgA was purified from the feces of healthy mice. Fecal samples were collected from multiple mice by dissecting the small and large intestine. The contents were pooled and mixed with 0.1% PBS-T and Roche protease inhibitor. The mixture was then vortexed vigorously for 5 minutes at maximum speed and clarified by centrifugation at 3000g for 10 minutes. The cleared supernatant was incubated with Pierce™ Protein L Magnetic Beads (Thermo Scientific) for 1 hour at constant shaking at room temperature. The beads were collected using a magnet separator and washed three times with 0.1% PBS-T. To elute the contents from the beads, 0.1M glycine at pH 2-2.5 was used, and the elution mixture was allowed to incubate for 10 minutes at room temperature. The beads were collected with the magnet, and the supernatant was retained. To neutralize the eluted material, 10% of the final elution volume of 1M Tris-HCl at pH 8 was added to the supernatant. The mixture was then passed through a 0.22 mm sterile filter, and its concentration was determined using a nanodrop.

Monoclonal IgA and structural variant generation

Recombinant SC, CR9114 SIgA, CR9914 IgA (monomeric IgA) and SFc□ (xFab) were produced following previously published methods[70]. Briefly, genes encoding the *mus musculus* IgA heavy chain constant region (Uniprot P01878) and the lambda light chain constant region (Uniprot A0A0G2JE99) were fused with the CR9114 VH and VL domain sequences[74] to create complete heavy chain and light chain sequences. Alternatively, the *mus musculus* IgA heavy chain constant region domains CH3 and CH4 were fused to an N-terminal hexahistine tag to create a Fcα expression construct. The TPA signal sequence (residues MDAMKRGLCCVLLLCGAVFVSPAGA) was encoded at the start of the heavy chain sequences and the mouse IgKappa signal sequence (residues METDTLLLWVLLLWVPGSTG) was encoded at the start of the light chain sequence. These sequences, along with *mus musculus* JC (Uniprot P01592; native signal peptide) and *mus musculus* pIgR ectodomain (SC) residues 1-567 (Uniprot O70570; native signal peptide) with C-terminal hexahistine affinity tag sequence, were cloned into mammalian expression vector pD2610v1 (Atum). Resulting expression constructs were transiently transfected or co-transfected into HEK Expi-293-F cells with the ExpiFectamine 293 transfection kit (ThermoFisher, A14525), according to company protocol. Resulting proteins were purified via CaptureSelect LC-lambda (mouse) affinity matrix (ThermoFisher, 194323010) or Ni-NTA agarose (Qiagen, 30210), and by Superose 6 Increase 10/300 GL (Cytiva Life Sciences, 29091596) size exclusion chromatography using an ÄKTA pure 25 chromatography system (Cytiva Life Sciences). Purified proteins were exchanged into 1x phosphate buffered saline buffer (HyClone, SH30258.01) prior to use in experiments.

Colon epithelial cell isolation

Mice were sacrificed by cervical dislocation. The colon was dissected on ice and opened longitudinally. Lumen content was gently removed and the tissue was washed 3 times in ice cold PBS. The mid colon was taken for further processing (a length of the tissue starting from 3 cm distal from the cecal junction and continuing for 4 cm toward the rectum). The tissue was cut into 1 cm pieces into PBS with 30 mM EDTA and 1.5 mM DTT and incubated on ice for 20 minutes with a brief shake at the end to remove mucus. The tissue was moved to DMEM with 30 mM EDTA and 2% fetal calf serum and incubated at 37C in a waterbath for 10 minutes with an aggressive shake for 30 seconds at the end to remove epithelial cells from the tissue. The cells in media were collected after passage through a metal sieve to remove remaining tissue. Pelleted cells were washed once with HBSS with 10% FCS then resuspended in HBSS (with divalent cations) with 2 mg/ml dispase II and incubated for 10 minutes at 37C in a water bath with brief shaking every 2 minutes to dissociate epithelia into a single cell solution (confirmed by light microscopy). The reaction was stopped by adding FCS to 10% and mixing by inversion. Cells were filtered through a 70 µm filter and washed with HBSS 10% FCS. Cells were stained for flow cytometry in complete T cell media: RPMI-1640 (Gibco 21870) plus 10% fetal bovine serum (Gibco10437), 1% Pen/Strep (Gibco15140), 1% L-glutamine (Gibco25030), 1% NaPyruvate (Gibco113690), 1% Nonessential amino acids (Gibco 11140), 1% HEPES (Gibco 15630) and 2-Mercaptoethanol [50uM] (Aldrich M6250), 1000x. For intracellular staining, cells were fixed, permeabilized, and stained using the eBioscience Foxp3 Transcription Factor Staining Buffer set according to the manufacturer's recommendations.

Single cell RNA-Seq

Epithelial cells isolated as described above (Colon epithelial cell isolation) were stained with individual Biolegend TotalSeq C antibodies (1:100) to allow for sample-level barcoding. Epithelial cells (SSC, FSC, live, CD45-, EPCAM+) were sorted on a BD FACSAria III Cell Sorter using a 70 µm nozzle at 45 psi, pooling 20,000 cells per sample together in one tube (total 120,000 cells). Post-sort viability was estimated to be 90% by trypan blue staining. A sample of the cell mixture was loaded into a single well of the 10X Genomics Chromium microfluidic device. A single-cell gene expression library was generated following the manufacturer's protocol for a Chromium Next GEM Single Cell 5' Reagent Kit v2 (Dual Index) with Feature Barcode technology for Cell Surface Protein (to capture the TotalSeq C sample barcodes). Libraries were sequenced on a NovaSeq S1 flow cell. Primary analysis, encompassing alignment and generation of feature barcodes matrices, was performed on Cell Ranger (v7.0.1), which showed 2,764 cells captured with a mean of 152,000 reads and 2,915 genes per cell. Cell Ranger was run with the option `--feature-ref=` to add the sequence information of the first six barcodes on TotalSeq C, the first three corresponding to $IgA^{+/-}$ samples and the last three to $IgA^{-/-}$ mice, according to the manufacturer recommendations. Filtered feature barcode matrices were then imported to the R environment using Seurat (v4.3.0) and all further analyses were done in R. Cells were filtered by singlet hashtag status, percentual of mitochondrial gene expression less than 10% and maximum RNA count per cell to avoid doublets and dying cells, then were scaled by SCT transform and all the PCA, UMAP and clustering possibilities were calculated. Final clustering resolution was decided according to biological difference between epithelial cell types and cell type annotation was performed using enrichment packages as ClusterProfiler (v4.6.2) and fgsea (v1.24.0) and manual curation. Differential Expression was perfomed using the FindMarkers function in Seurat. Graphs were plotted using Seurat functions, iSEE visualization package (v2.10.0) and ggplot2 (v3.4.3). Final functional enrichment for figures was done using fgsea (v1.24.0) against GO BP and msigdb mice c2 databases(c2.cgp.v7.5.1.symbols and c5.go.bp.v7.5.1.symbols).

Measurements of epithelial proliferation (EdU, Ki67, pERK)

Mice received 500 µg of 5-ethynyl 2'-deoxyuridine (EdU) (Thermo Fisher A10044) in a 100 µl PBS intraperitoneal injection at 24 hours and 4 hours prior to sacrifice. The colon was dissected on ice, opened longitudinally, and lumen content was gently removed with forceps. Swiss rolls of colon tissue were fixed in PBS-buffered 2% PFA for 2 hours at 4C, washed three times with PBS, and frozen in OCT. A cryostat was used to cut 16 µm sections which were adhered to Superfrost Plus White slides (Fisherbrand). Edu was visualized using the Click-iT EdU Alexa Fluor 647 Imaging Kit (Thermo Fisher) according to the manufacturer's protocol, including a counterstain with 1:200 AF488 anti-mouse CD326 (EPCAM) (Biolegend Cat#118210). Stained sections were mounted with Fluoromount G (Southern Biotech) and imaged on a Keyence BZ-X800

epifluorescence microscope. Crypts were assessed in the mid-colon region (only the middle third of the length of the colon) and only counted when both the bottom and top of the same crypt was clearly discernable by EPCAM staining. At least 5 fields of view and at least 20 crypts were counted for each sample. For Ki67 staining, epithelial cells were prepared from mid colon samples as described above (Colon epithelial cell isolation) and analyzed on a BD FACSymphony. Phosphorylated ERK was measured by preparing epithelial cells as described above (Colon epithelial cell isolation) and using a Phospho-Erk1 (pThr202 / pTyr204 + Erk2 (pTyr185/187) and pan-Erk1 / 2 ELISA Kit from Sigma (Cat. RAB0349) according to manufacturer's instructions.

Isolation and culture of mouse-derived colon organoids

Crypts were isolated from the colons of IgA knockout mice through successive 30-minute and 1-hour incubations at 4°C in PBS containing 10 mM EDTA, according to a published method[75]. Following isolation, the cells were immersed in a hybrid medium consisting of 50% primary medium, which was composed of DMEM/F12 and supplemented with 1% HEPES (Gibco 15630), 1% L-glutamine (Gibco25030), 1% Pen/Strep (Gibco15140), and 20% fetal bovine serum (Gibco10437), and 50% conditioned L-WRN medium, enriched with 50 ng/mL EGF [500µg/mL] (Sigma SPR 3196-500). Cells were mixed with Matrigel (Fisher Scientific CB40230C) (30-50%) and dispensed into a 48-well plate at 200 µL per well, being incubated for 20 minutes at 37°C. Afterward, 300 µL of enriched hybrid media was added to each well. The media was changed after 3 days, and organoids were split after an additional 2 days. For passaging, organoids were dissociated by incubation in TrypLE Express Enzyme (1X), Phenol Red (Thermo Scientific 12605010). For subsequent culture, the cells were placed in the enriched hybrid media mixed with matrigel (30-50%). A volume of 40 µL of the cell-matrigel suspension was dispensed into 5 distributed drops per well in a 6-well plate. The plate was incubated to polymerize the matrigel at 37°C for 5 minutes and then inverted to prevent cell attachment to the bottom of the plate surface. Treatments with antibodies, including IgA purified from feces and mouse IgG2a isotype control (BioXCell BE0085), were embedded in supplemented hybrid media and placed in their respective wells. The media was changed after 3 days. Imaging was performed for 4-5 days after adding treatments using Z-stack on a Keyence BZ-X800 epifluorescence microscope. Image quantifications were made in ImageJ 2.14.0 and Tellu[76], and all image calculations were made in R studio 4.2.2.

Statistical methods

Unless otherwise state, mean and standard error are plotted for all figures. For comparisons between two groups, two-tailed Mann-Whitney tests were performed. For three or more groups, Kruskal-Wallis tests were performed with Dunn's correction for multiple comparisons. Exact p values are reported on graphs for Mann-Whitney and Kruskal-Wallis tests when the p value or adjusted p value is less than 0.1. For sequencing analyses, application-specific statistical methods are described in the respective methods sections or figure legends.

Data Availability

All raw sequencing data for bulk RNA-Seq, 16S rRNA amplicon sequencing, and single cell RNA-Seq are available on the NCBI Sequence Read Archive (SRA) under a unified project: PRJNA1023250.

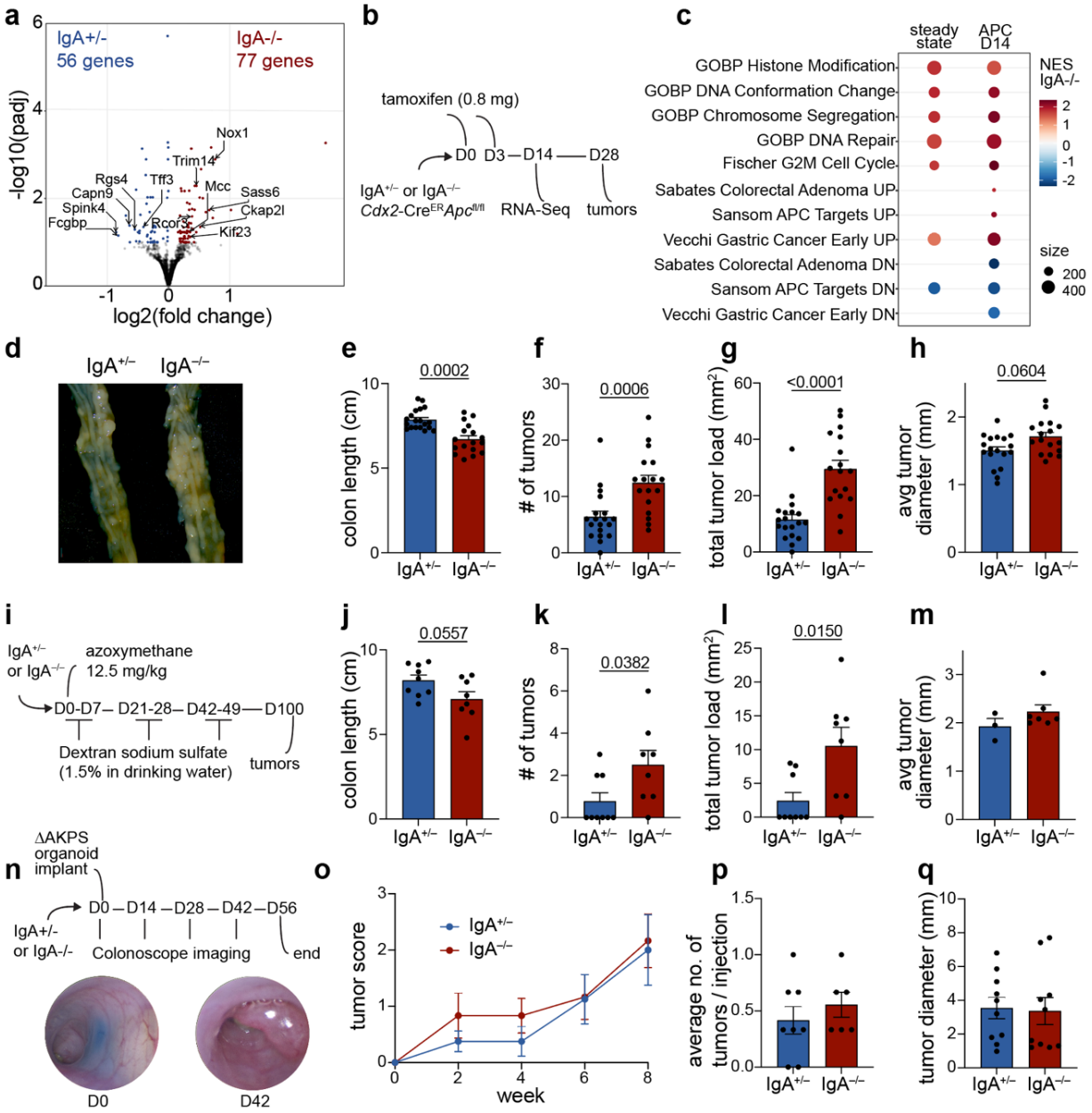

Fig. 1 | IgA$^{-/-}$ mice have pro-tumor alterations to colon tissue and increased susceptibility to endogenous colorectal cancer models. a, Bulk RNA-Seq of colon tissue from IgA$^{+/-}$ and IgA$^{-/-}$ mice during steady state revealed upregulation of transit-amplifying cell markers and downregulation of goblet cell markers (n = 5). **b**, Experimental design for studies of IgA in the context of epithelial-specific loss of *APC*. **c**, Gene set enrichment analyses indicated a pro-cancerous phenotype of IgA$^{-/-}$ mice that was exacerbated after APC loss (n = 5 steady, 4 APC, visible dots only for gene sets where adjusted $p < 0.05$). **d-h**, On day 28, mice were sacrificed and assessed for colon length, number of colon tumors, total tumor load, and average tumor size (n = 19, 17). **i**, Experimental design for azoxymethane (AOM) and dextran sodium sulfate (DSS) model of colorectal cancer. **j-m**, Mice were sacrificed at day 100 to assess tumor outcomes as in **e-h** (n = 9, 8 except panel m includes only mice with tumors: n = 3, 7). **n**, Experimental design and example images for colonoscope-guided implant of quadruple-knockout (*APC*, *Kras*, *P53*, *Smad4*) organoid cells. **o**, Tumor growth was tracked longitudinally by colonoscope and scored based on the size of the tumor relative to the colon circumference (n = 8, 6, details in methods). **p**, After 8 weeks, mice were sacrificed to assess the average number of tumors per injection (not all injections result in implantation) and **q**, tumor size (n = 10). (Mann-Whitney, p values hidden when $p > 0.1$)

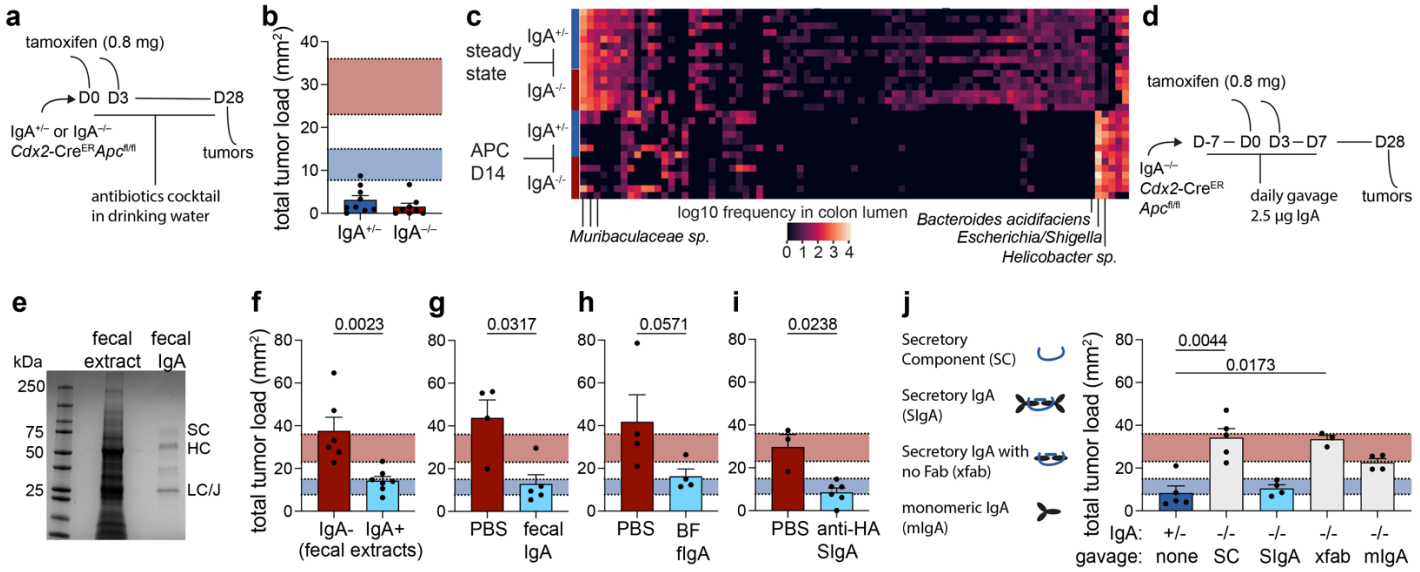

Fig. 2 | Role of the microbiome and IgA structure in tumorigenesis. a, Experimental design for broad spectrum antibiotic treatment (ampicillin, vancomycin, neomycin, metronidazole) to assess role of microbiome in tumor development in the context of IgA deficiency and *APC* loss. **b**, Total tumor load was dramatically reduced by antibiotic treatment in both $IgA^{+/-}$ and $IgA^{-/-}$ mice to similar levels (n = 9, 8). **c**, Heatmap of amplicon sequence variants (columns) identified in colon lumen samples from indicated mice (rows) demonstrates dramatic shift caused by *APC* loss, but no effect of IgA (n = 9, 6, 7, 6). **d**, Experimental design for gavage treatments to prevent tumorigenesis in $IgA^{-/-}$ mice in the context of *APC* loss. **e**, Denaturing gel of sterile fecal extract and resulting purified fecal IgA. **f-h**, Total tumor load following *APC* loss in $IgA^{-/-}$ mice treated with **f**, indicated sterile fecal extracts from healthy donor mice (n = 6), **g**, purified fecal IgA from healthy donor mice (n = 4, 5), or **h**, purified fecal IgA from germfree mice mono-colonized with *Bacteroides fragilis* (n = 4). **i-j**, Total tumor load following *APC* loss in $IgA^{-/-}$ mice treated with **i**, recombinant CR9114 anti-influenza HA secretory IgA (n = 3, 6) or **j**, structural variations thereof (n = 5, 5, 4, 3, 4). (Shaded areas in tumor load plots represent the 95% confidence interval of tumor load for $IgA^{+/-}$, blue, and $IgA^{-/-}$, red, mice from Fig. 1, Mann-Whitney, p values hidden when $p > 0.1$)

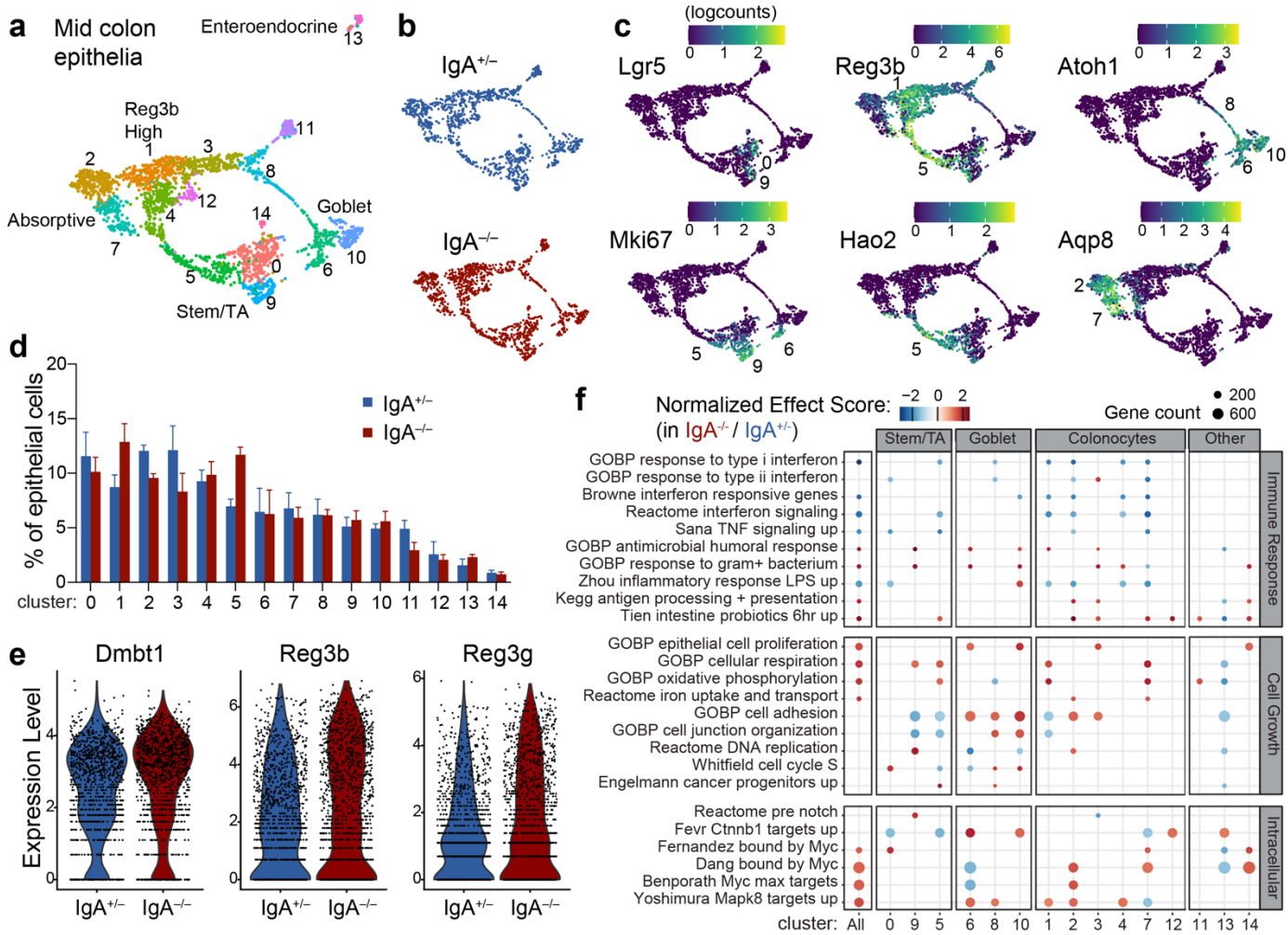

Fig. 3 | Cellular changes in the colon epithelium of IgA$^{-/-}$ mice. a, UMAP and clustering of sorted single colon epithelial cell (live, CD45-, EPCAM+) transcriptomes from **b**, IgA$^{+/-}$ and IgA$^{-/-}$ littermates (n = 3 mice per group). **c**, Example markers used to identify clusters: *Lgr5* (stem), *Mki67* (cycling), *Reg3b* (antimicrobial function), *Hao2* (absorptive progenitor), *Atoh1* (secretory progenitor), *Aqp8* (absorptive colonocyte). **d**, Proportion of cells in each cluster by genotype. **e**, Expression of example antimicrobial-encoding genes induced across all cells in IgA$^{-/-}$ mice. **f**, Gene set enrichment analyses across all cells and within individual clusters based on IgA genotype revealed a switch from interferon signaling to anti-bacterial pathways, increases in cell cycling, and alterations in intracellular signaling processes. Dots are visible where adjusted p value < 0.05, size of dot represents the number of genes in the pathway, and color represents the normalized enrichment score of that pathway (IgA$^{-/-}$-enriched is positive, red).

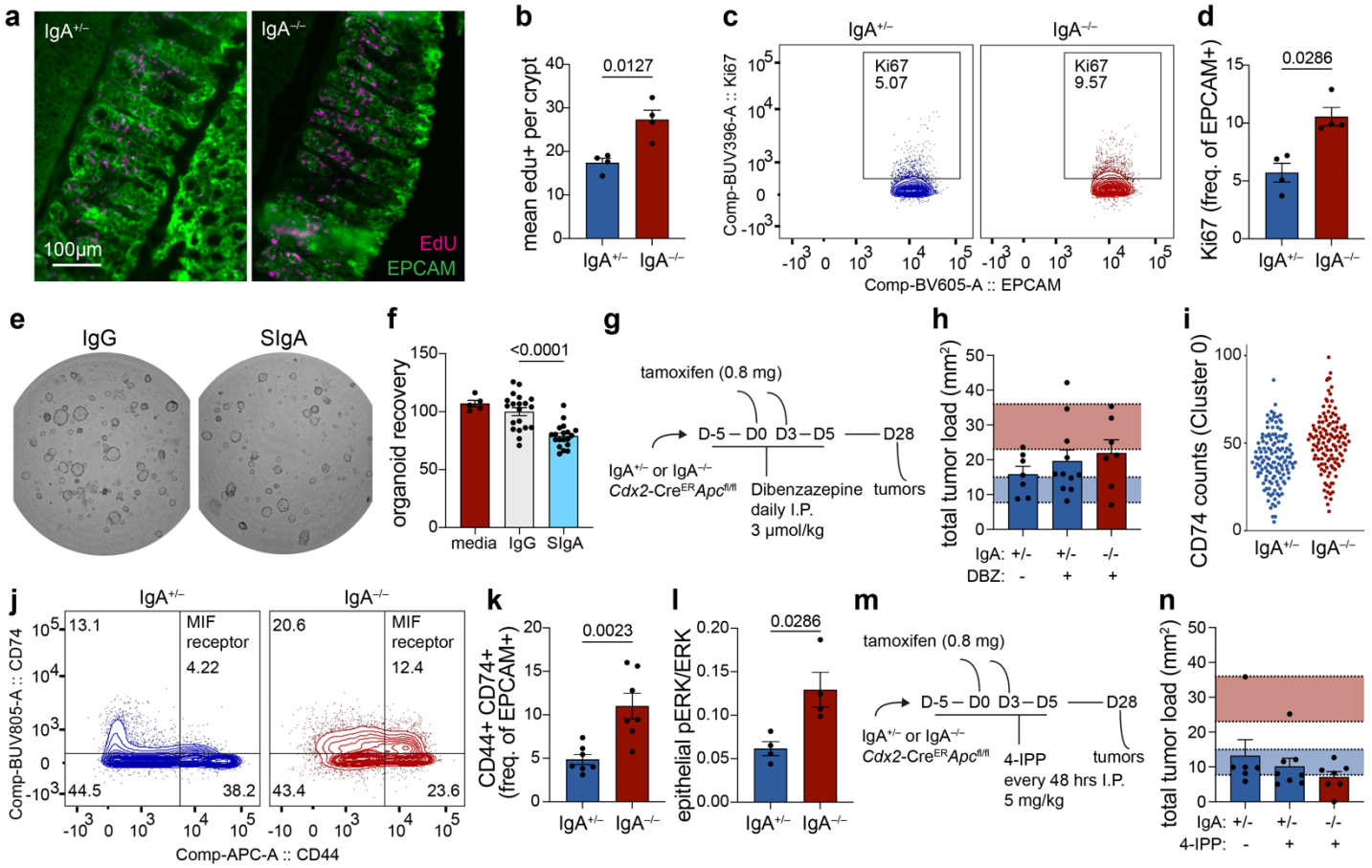

Fig. 4 | Epithelial proliferation is suppressed by IgA, which consequently reduces tumorigenesis. a, Fluorescence microscopy of frozen sections of swiss-rolled mid-colon from mice injected with EdU at 24 and 4 hours prior. **b**, Quantification of EdU positive cells per crypt, averaged across at least 20 crypts and 5 frames of view per animal (n = 4). **c**, Flow cytometry of colon epithelial cells (CD45-, EPCAM+) with intracellular staining of the cell cycle marker Ki67. **d**, Quantification of the frequency of Ki67+ epithelial cells depending on IgA genotype (n = 4). **e**, Primary mouse colon organoids were cultured from isolated crypts in the presence of indicated antibody isotypes imaged by brightfield microscopy. **f**, Organoid counting from four independent experiments pooled and normalized to the IgG treatment control (n = 5, 20, 19). **g**, Experimental design for Notch inhibition to suppress epithelial proliferation in the context of IgA deficiency and *APC* loss, which was assessed by **h**, total tumor load (n = 7, 11, 7). **i**, CD74 expression level in cluster 0 stem cells from the single cell transcriptome data of Fig. 3. **j**, Flow cytometry analysis of surface MIF receptor (CD44/CD74) in colon epithelial cells revealed **k**, increased surface CD74 and MIF receptor on cells from $IgA^{-/-}$ animals (n = 6, 7). **l**, ELISA of lysate of isolated colon epithelial cells specific for phosphorylated ERK normalized to the level of total ERK (n = 4). **m**, Experimental design for MIF inhibitor treatment in the context of IgA deficiency and *APC* loss. **n**, MIF inhibition did not alter the total tumor load in $IgA^{+/-}$ mice but did reduce tumor burden in $IgA^{-/-}$ mice to the control level (n = 6, 8, 7). (Shaded areas in tumor load plots represent the 95% confidence interval of tumor load for $IgA^{+/-}$, blue, and $IgA^{-/-}$, red, mice from Fig. 1, Mann-Whitney, p values hidden when $p > 0.1$)

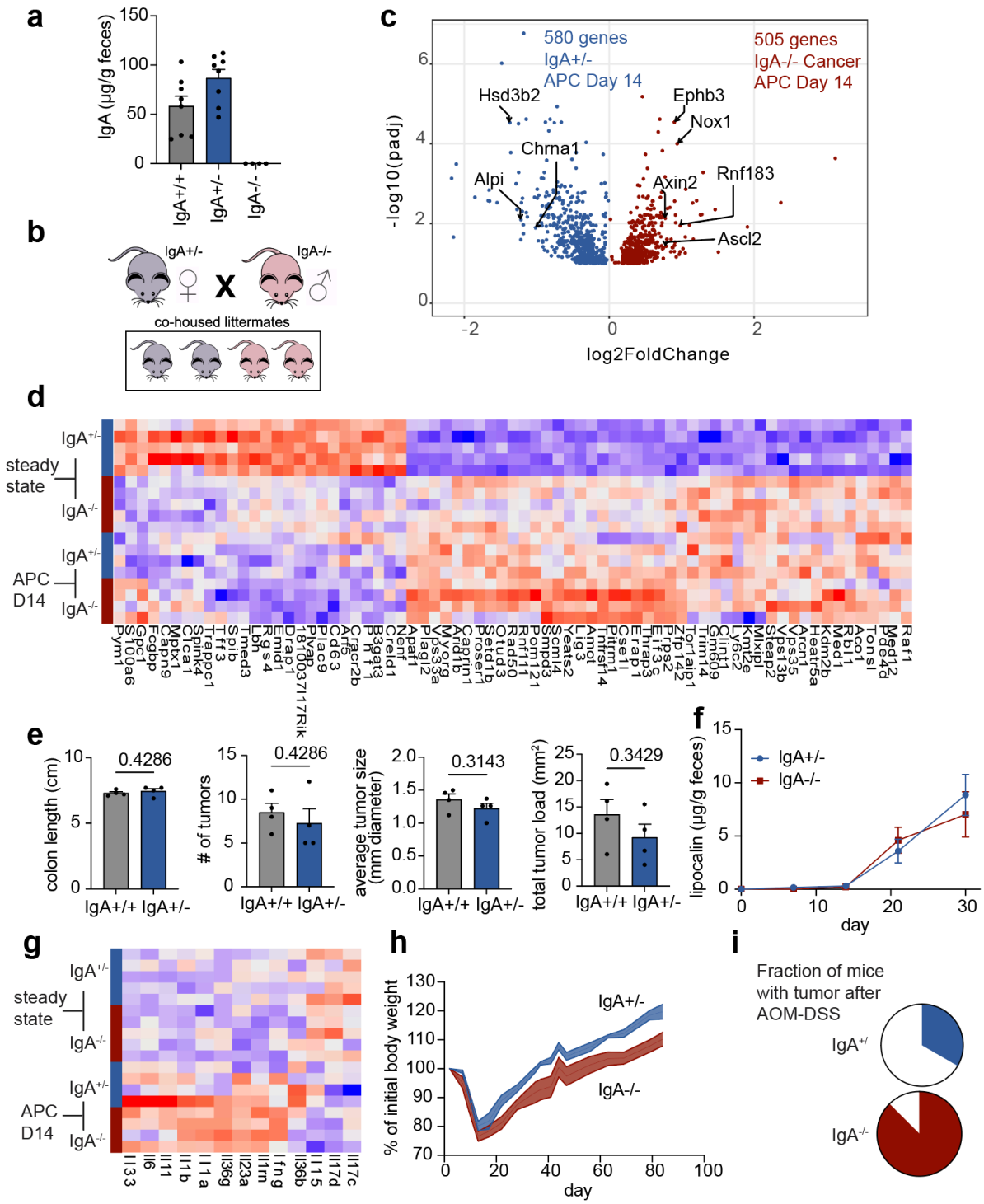

Extended Data Fig. 1 | Additional data related to Fig. 1. a, ELISA of fecal IgA in homozygotes and heterozygotes of the IgA$^{-/-}$ strain crossed with C57BL6/J (n = 8, 8, 4). **b**, Breeding scheme for littermate controls. **c**, Differentially expressed genes in bulk RNA-Seq from mid-colon tissue of IgA$^{+/-}$ and IgA$^{-/-}$ littermates fourteen days after inducing colon epithelial-specific loss of *APC* (n = 4). **d**, Set of genes identified as modulated by both *APC* loss (steady state vs. APC Day 14 comparison) and IgA deficiency at steady state (IgA$^{+/-}$ vs. IgA$^{-/-}$). Interestingly, the direction of the effect of IgA deficiency is toward the direction caused by *APC* loss (n = 5, 5, 4, 4). **e**, Endpoint analyses of the APC-driven cancer model using IgA$^{+/+}$ and IgA$^{+/-}$ littermates (n = 4). **f**, ELISA for fecal lipocalin in the APC-driven cancer model (n = 3, from one cohort, representative). **g**, Cytokine gene expression in the bulk colon tissue RNA-Seq shows no IgA-dependent alterations in inflammatory pathways (n = 5, 5, 4, 4). **h**, Body weight change during AOM-DSS (n = 4, from one cohort, representative). **i**, Tumor frequency in the AOM-DSS cancer model (n = 9, 8).

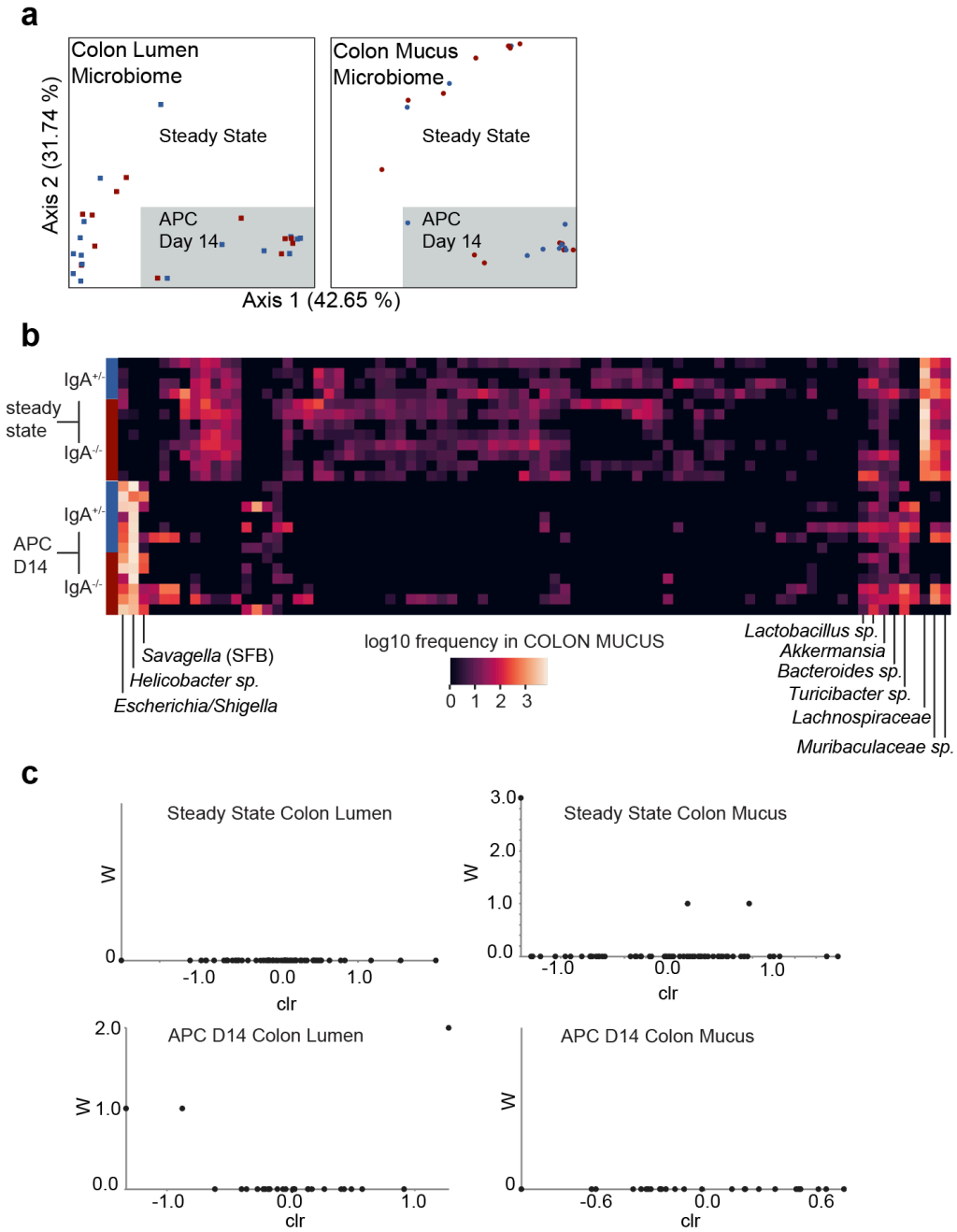

Extended Data Fig. 2 | Additional microbiome profiling data. a, Beta diversity (weighted unifrac distance) of microbiome measured by 16S rRNA amplicon sequencing of samples from IgA$^{+/-}$ (blue) and IgA$^{-/-}$ (red) mice showing no genotype-specific alterations (lumen n = 9, 6, 7, 6, mucus n = 4, 8, 7, 6). **b**, Heatmap of amplicon sequence variants (columns) identified in colon mucus samples from indicated mice (rows) demonstrates dramatic shift caused by *APC* loss, but no effect of IgA. **c**, ANCOM differential abundance testing of IgA$^{+/-}$ vs. IgA$^{-/-}$ littermates in the indicated sample types identified no IgA-dependent alterations in the microbiome.

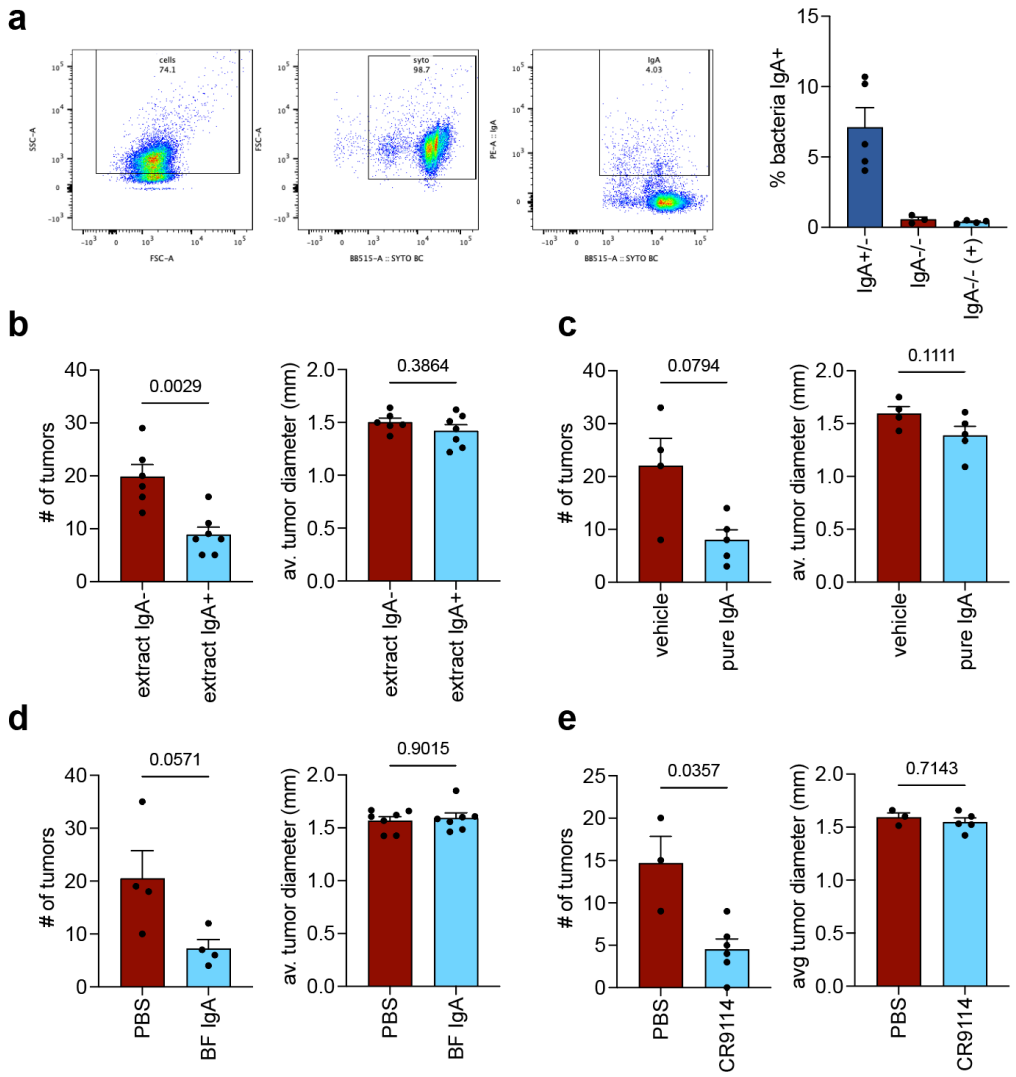

Extended Data Fig. 3 | Additional results related to IgA gavage treatments. a, Gating strategy for flow cytometry for IgA coating of bacterial cells in fecal samples and summary data showing a lack of IgA binding to bacteria when IgA$^{-/-}$ mice were gavaged with fecal IgA purified from germfree mice monocolonized with *Bacteroides fragilis* (n = 5, 3, 4). **b-e**, Counts and sizes of tumors from IgA$^{-/-}$ mice treated with **b**, fecal extracts (n = 6, 7), **c**, purified fecal IgA from SPF mice (n = 4, 5), **d**, purified fecal IgA from mice mono-colonized with *Bacteroides fragilis* (n = 4), or **e**, recombinant CR9114 anti-influenza HA monoclonal secretory IgA (n = 3, 5).

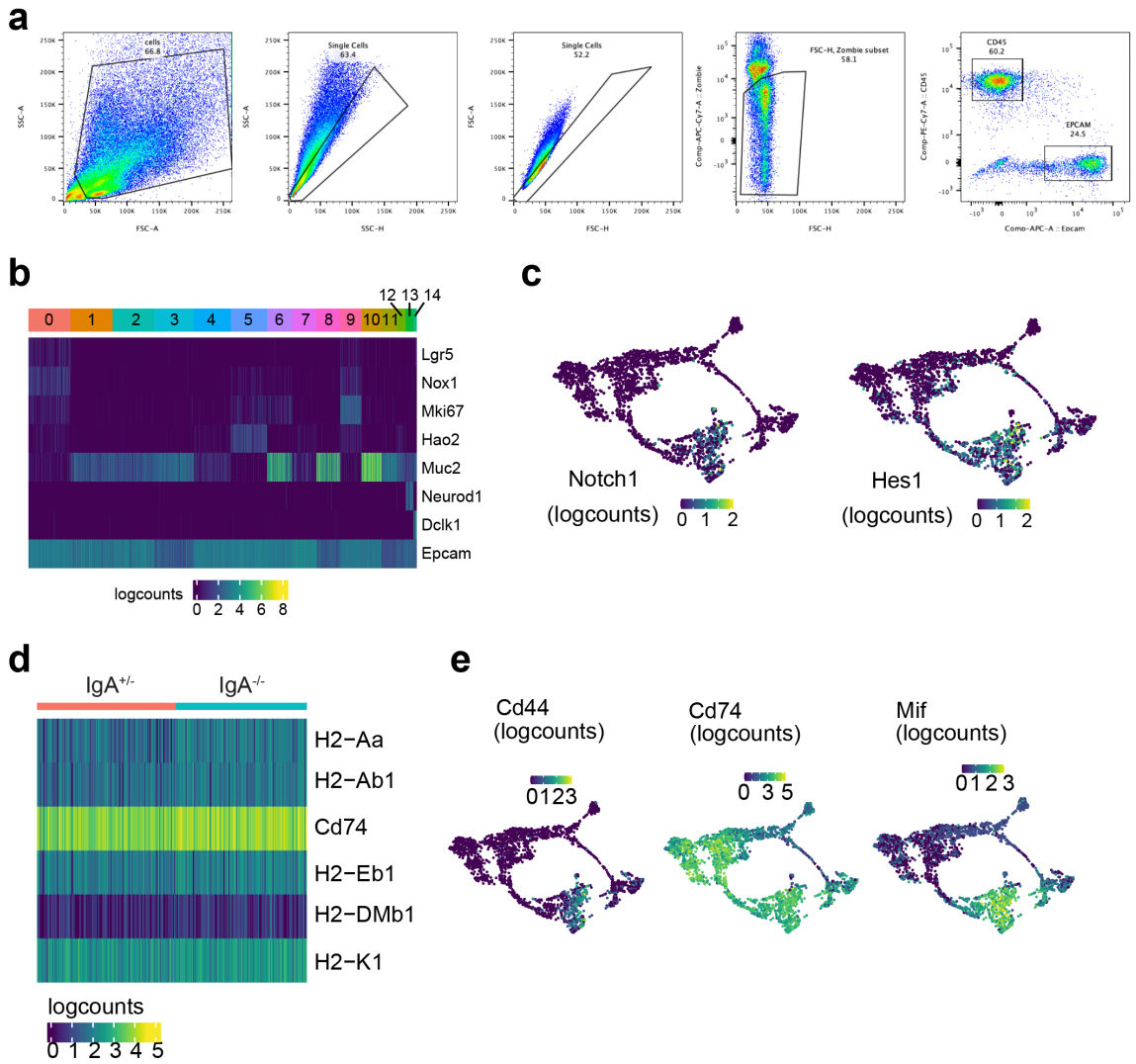

Extended Data Fig. 4 | Additional data related to colon epithelial single cell RNA-Seq. a, Gating strategy for sorting live EPCAM+, CD45- epithelial cells for single-cell transcriptomics (n = 3). **b**, Various markers to aid in identifying clusters: *Lgr5* (stem), *Nox1* (transit-amplifying), *Mki67* (cycling), *Hao2* (immature), *Muc2* (low: mature, high: goblet), *Neurod1* (enteroendocrine), *Dclk1* (Tuft), and *Epcam* (pan-epithelial). **c**, Notch pathway-related markers. **d**, altered MHCII genes in cluster 0. **e**, MIF signaling components are co-expressed in the stem cells.

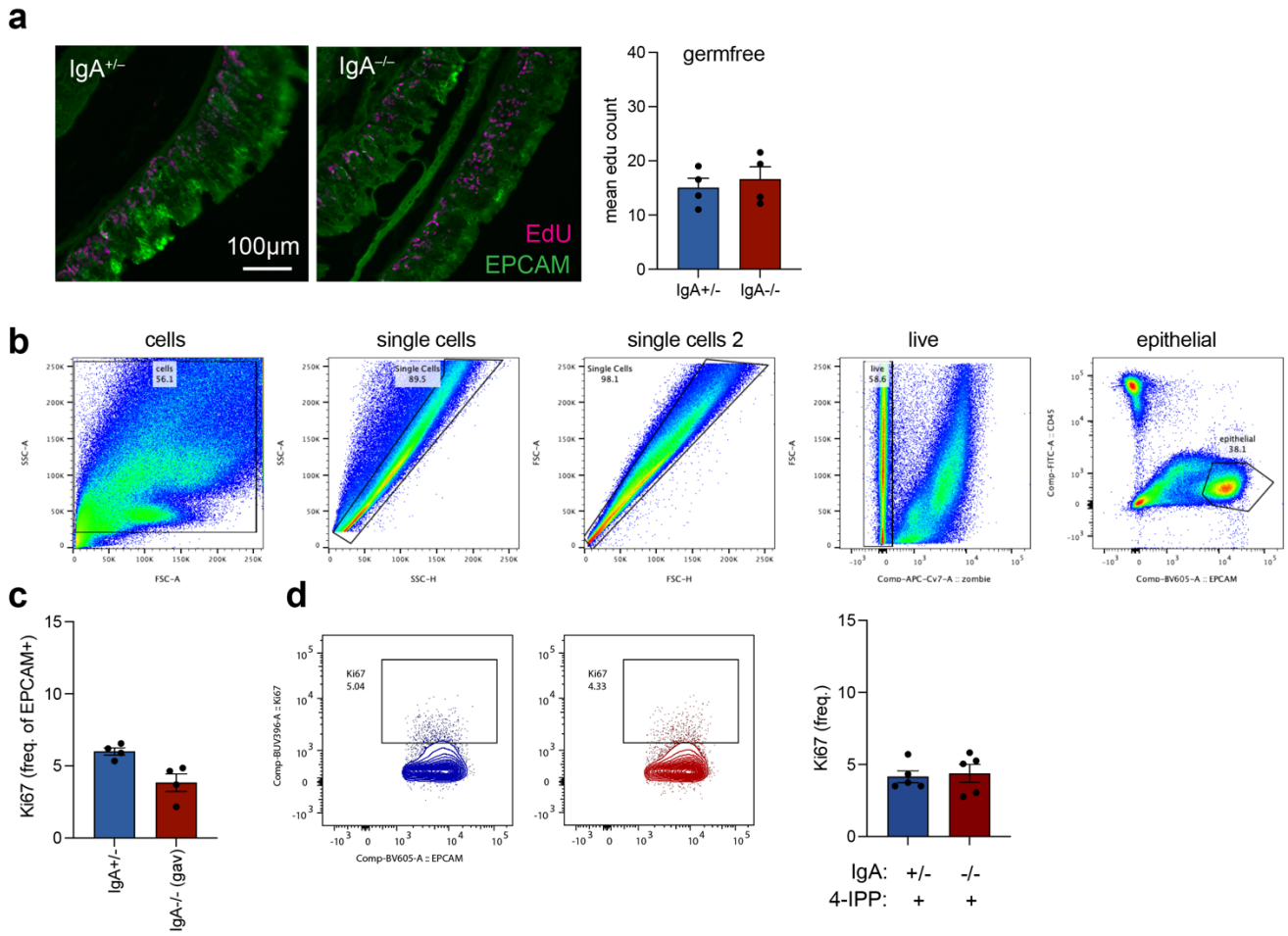

Extended Data Fig. 5 | Additional data related to epithelial proliferation. a, EdU (pink) and EPCAM (green) staining in germfree mice after two injections (-24 hours and -4 hours) of EdU showed no difference between $IgA^{+/-}$ and $IgA^{-/-}$ littermates (n = 4). **b**, Gating strategy for analyzing EPCAM+, CD45- epithelial cells for intracellular staining of Ki67 or surface staining of MIF receptor. **c**, Intracellular Ki67 staining of EPCAM+CD45- epithelial cells from mid-colon of $IgA^{+/-}$ mice and $IgA^{-/-}$ littermates that were gavaged daily for 5 days with anti-HA influenza monoclonal secretory IgA (n = 4). **d**, The same analysis of $IgA^{+/-}$ mice and $IgA^{-/-}$ littermates that were both treated with the selective MIF inhibitor 4-IPP for 10 days (every 48 hours, n = 4, 5).

References

1. Fagarasan, S. Evolution, development, mechanism and function of IgA in the gut. *Curr. Opin. Immunol.* **20**, 170–177 (2008).

2. Pabst, O. & Slack, E. IgA and the intestinal microbiota: the importance of being specific. *Mucosal Immunol.* **13**, 12–21 (2020).

3. Huus, K. E., Petersen, C. & Finlay, B. B. Diversity and dynamism of IgA−microbiota interactions. *Nat Rev Immunol* 1–12 (2021) doi:10.1038/s41577-021-00506-1.

4. Catanzaro, J. R. *et al.* IgA-deficient humans exhibit gut microbiota dysbiosis despite secretion of compensatory IgM. *Scientific reports* **9**, 13574–10 (2019).

5. Yel, L. Selective IgA deficiency. *Journal of clinical immunology* (2010) doi:10.1007/s10875-009-9357-x.

6. Fadlallah, J. *et al.* Microbial ecology perturbation in human IgA deficiency. *Science Translational Medicine* **10**, eaan1217 (2018).

7. Conrey, P. E. *et al.* IgA deficiency destabilizes homeostasis toward intestinal microbes and increases systemic immune dysregulation. *Sci Immunol* **8**, eade2335 (2023).

8. Moll, J. M. *et al.* Gut microbiota perturbation in IgA deficiency is influenced by IgA-autoantibody status. *Gastroenterology* (2021) doi:10.1053/j.gastro.2021.02.053.

9. Shroff, K. E., Meslin, K. & Cebra, J. J. Commensal enteric bacteria engender a self-limiting humoral mucosal immune response while permanently colonizing the gut. *Infection and immunity* **63**, 3904–3913 (1995).

10. Singh, K., Chang, C. & Gershwin, M. E. IgA deficiency and autoimmunity. *Autoimmunity reviews* **13**, 163–177 (2014).

11. Ludvigsson, J. F., Neovius, M., Ye, W. & Hammarström, L. IgA deficiency and risk of cancer: a population-based matched cohort study. *Journal of clinical immunology* **35**, 182–188 (2015).

12. Langford, T. D. *et al.* Central Importance of Immunoglobulin A in Host Defense against Giardia spp. *Infect Immun* **70**, 11–18 (2002).

13. Blutt, S. E., Miller, A. D., Salmon, S. L., Metzger, D. W. & Conner, M. E. IgA is important for clearance and critical for protection from rotavirus infection. *Mucosal immunology* **5**, 712–719 (2012).

14. Moor, K. *et al.* High-avidity IgA protects the intestine by enchaining growing bacteria. *Nature* **544**, 498–502 (2017).

15. Jørgensen, S. F. *et al.* Selective IgA deficiency in humans is associated with reduced gut microbial diversity. *The Journal of allergy and clinical immunology* **143**, 1969-1971.e11 (2019).

16. Gatti, R. A. & Good, R. A. Occurrence of malignancy in immunodeficiency diseases: A literature review. *Cancer* **28**, 89–98 (1971).

17. Filipovich, A. H., Mathur, A., Kamat, D., Kersey, J. H. & Shapiro, R. S. Lymphoproliferative disorders and other tumors complicating immunodeficiencies. *Immunodefic* **5**, 91–112 (1994).

18. Tjalsma, H., Boleij, A., Marchesi, J. R. & Dutilh, B. E. A bacterial driver–passenger model for colorectal cancer: beyond the usual suspects. *Nat Rev Microbiol* **10**, 575–582 (2012).

19. Cullin, N., Antunes, C. A., Straussman, R., Stein-Thoeringer, C. K. & Elinav, E. Microbiome and cancer. *Cancer Cell* (2021) doi:10.1016/j.ccell.2021.08.006.

20. Clay, S. L., Fonseca-Pereira, D. & Garrett, W. S. Colorectal cancer: the facts in the case of the microbiota. *J Clin Invest* **132**, e155101 (2022).

21. Ludvigsson, J. F., Neovius, M. & Hammarström, L. IgA Deficiency & Mortality: A Population-Based Cohort Study. *J Clin Immunol* **33**, 1317–1324 (2013).

22. Cunningham-Rundles, C., Pudifin, D. J., Armstrong, D. & Good, R. A. Selective IgA Deficiency and Neoplasia. *Vox Sang* **38**, 61–67 (1980).

23. Pulvirenti, F. *et al.* Gastric Cancer Is the Leading Cause of Death in Italian Adult Patients With Common Variable Immunodeficiency. *Front Immunol* **9**, 2546 (2018).

24. Shulzhenko, N. *et al.* Crosstalk between B lymphocytes, microbiota and the intestinal epithelium governs immunity versus metabolism in the gut. *Nature medicine* **17**, 1585–1593 (2011).

25. Kawamoto, S. *et al.* The inhibitory receptor PD-1 regulates IgA selection and bacterial composition in the gut. *Science* **336**, 485–489 (2012).

26. Kubinak, J. L. *et al.* MyD88 signaling in T cells directs IgA-mediated control of the microbiota to promote health. *Cell host & microbe* **17**, 153–163 (2015).

27. Suzuki, K. *et al.* Aberrant expansion of segmented filamentous bacteria in IgA-deficient gut. *Proceedings of the National Academy of Sciences of the United States of America* **101**, 1981–1986 (2004).

28. Fagarasan, S. *et al.* Critical roles of activation-induced cytidine deaminase in the homeostasis of gut flora. *Science* **298**, 1424–1427 (2002).

29. Gopalakrishna, K. P. *et al.* Maternal IgA protects against the development of necrotizing enterocolitis in preterm infants. *Nat Med* **25**, 1110–1115 (2019).

30. Kawamoto, S. *et al.* Foxp3(+) T cells regulate immunoglobulin a selection and facilitate diversification of bacterial species responsible for immune homeostasis. *Immunity* **41**, 152–165 (2014).

31. Nagashima, K. *et al.* Identification of subepithelial mesenchymal cells that induce IgA and diversify gut microbiota. *Nat Immunol* **18**, 675–682 (2017).

32. Bunker, J. J. *et al.* Natural polyreactive IgA antibodies coat the intestinal microbiota. *Science* **358**, eaan6619 (2017).

33. Shimoda, M., Inoue, Y., Azuma, N. & Kanno, C. Natural polyreactive immunoglobulin A antibodies produced in mouse Peyer's patches. *Immunity* **97**, 9–17 (1999).

34. Rollenske, T. *et al.* Cross-specificity of protective human antibodies against Klebsiella pneumoniae LPS O-antigen. *Nature immunology* **19**, 617–624 (2018).

35. Kabbert, J. *et al.* High microbiota reactivity of adult human intestinal IgA requires somatic mutations. *The Journal of experimental medicine* **217**, (2020).

36. Nowosad, C. R. *et al.* Tunable dynamics of B cell selection in gut germinal centres. *Nature* **588**, 321–326 (2020).

37. Peterson, D. A. *et al.* Characterizing the Interactions Between a Naturally-primed Immunoglobulin A and its Conserved Bacteroides thetaiotaomicron Species-specific Epitope in Gnotobiotic Mice. *The Journal of biological chemistry* (2015) doi:10.1074/jbc.m114.633800.

38. Nakajima, A. *et al.* IgA regulates the composition and metabolic function of gut microbiota by promoting symbiosis between bacteria. *The Journal of experimental medicine* **67**, jem.20180427-2034 (2018).

39. Donaldson, G. P. *et al.* Gut microbiota utilize immunoglobulin A for mucosal colonization. *Science* **360**, 795–800 (2018).

40. Rollenske, T. *et al.* Parallelism of intestinal secretory IgA shapes functional microbial fitness. *Nature* 1–5 (2021) doi:10.1038/s41586-021-03973-7.

41. Harriman, G. R. *et al.* Targeted deletion of the IgA constant region in mice leads to IgA deficiency with alterations in expression of other Ig isotypes. *The Journal of Immunology* **162**, 2521–2529 (1999).

42. Murthy, A. K., Dubose, C. N., Banas, J. A., Coalson, J. J. & Arulanandam, B. P. Contribution of polymeric immunoglobulin receptor to regulation of intestinal inflammation in dextran sulfate sodium-induced colitis. *Journal of gastroenterology and hepatology* **21**, 1372–1380 (2006).

43. Mathias, A. & Corthésy, B. N-Glycans on secretory component: mediators of the interaction between secretory IgA and gram-positive commensals sustaining intestinal homeostasis. *Gut microbes* **2**, 287–293 (2011).

44. Kaetzel, C. S. The polymeric immunoglobulin receptor: bridging innate and adaptive immune responses at mucosal surfaces. *Immunol. Rev.* **206**, 83–99 (2005).

45. Ramanan, D. *et al.* An Immunologic Mode of Multigenerational Transmission Governs a Gut Treg Setpoint. *Cell* **181**, 1276-1290.e13 (2020).

46. Robertson, S. J. *et al.* Comparison of Co-housing and Littermate Methods for Microbiota Standardization in Mouse Models. *Cell Rep.* **27**, 1910-1919.e2 (2019).

47. Donaldson, G. P., Lee, S. M. & Mazmanian, S. K. Gut biogeography of the bacterial microbiota. *Nature reviews. Microbiology* **14**, 20–32 (2015).

48. Post, S. van der, Birchenough, G. M. H. & Held, J. M. NOX1-dependent redox signaling potentiates colonic stem cell proliferation to adapt to the intestinal microbiota by linking EGFR and TLR activation. *Cell Reports* **35**, 108949 (2021).

49. Grivennikov, S. I. *et al.* Adenoma-linked barrier defects and microbial products drive IL-23/IL-17-mediated tumour growth. *Nature* **491**, 254–258 (2012).

50. Grivennikov, S. I. Inflammation and colorectal cancer: colitis-associated neoplasia. *Seminars in immunopathology* **35**, 229–244 (2013).

51. Mandal, S. *et al.* Analysis of composition of microbiomes: a novel method for studying microbial composition. *Microb. Ecol. Heal. Dis.* **26**, 27663 (2015).

52. Beumer, J. & Clevers, H. Cell fate specification and differentiation in the adult mammalian intestine. *Nat. Rev. Mol. Cell Biol.* **22**, 39–53 (2021).

53. Tsang, D. K. L. *et al.* A single cell survey of the microbial impacts on the mouse small intestinal epithelium. *Gut Microbes* **14**, 2108281 (2022).

54. Rakoff-Nahoum, S., Paglino, J., Eslami-Varzaneh, F., Edberg, S. & Medzhitov, R. Recognition of Commensal Microflora by Toll-Like Receptors Is Required for Intestinal Homeostasis. *Cell* **118**, 229–241 (2004).

55. Sato, T. *et al.* Single Lgr5 stem cells build crypt-villus structures in vitro without a mesenchymal niche. *Nature* **459**, 262–265 (2009).

56. Merenda, A., Fenderico, N. & Maurice, M. M. Wnt Signaling in 3D: Recent Advances in the Applications of Intestinal Organoids. *Trends Cell Biol.* **30**, 60–73 (2020).

57. Fre, S. *et al.* Notch signals control the fate of immature progenitor cells in the intestine. *Nature* **435**, 964–968 (2005).

58. Es, J. H. van *et al.* Notch/γ-secretase inhibition turns proliferative cells in intestinal crypts and adenomas into goblet cells. *Nature* **435**, 959–963 (2005).

59. Biton, M. *et al.* T Helper Cell Cytokines Modulate Intestinal Stem Cell Renewal and Differentiation. *Cell* **175**, 1307-1320.e22 (2018).

60. Koyama, M. *et al.* MHC Class II Antigen Presentation by the Intestinal Epithelium Initiates Graft-versus-Host Disease and Is Influenced by the Microbiota. *Immunity* **51**, 885-898.e7 (2019).

61. Leng, L. *et al.* MIF Signal Transduction Initiated by Binding to CD74. *J. Exp. Med.* **197**, 1467–1476 (2003).

62. Shi, X. *et al.* CD44 Is the Signaling Component of the Macrophage Migration Inhibitory Factor-CD74 Receptor Complex. *Immunity* **25**, 595–606 (2006).

63. Pelka, K. *et al.* Spatially organized multicellular immune hubs in human colorectal cancer. *Cell* **184**, 4734-4752.e20 (2021).

64. Farr, L. *et al.* CD74 Signaling Links Inflammation to Intestinal Epithelial Cell Regeneration and Promotes Mucosal Healing. *Cell Mol Gastroenterology Hepatology* **10**, 101–112 (2020).

65. Winner, M. *et al.* A Novel, Macrophage Migration Inhibitory Factor Suicide Substrate Inhibits Motility and Growth of Lung Cancer Cells. *Cancer Res.* **68**, 7253–7257 (2008).

66. Biswas, S. *et al.* IgA transcytosis and antigen recognition govern ovarian cancer immunity. *Nature* **591**, 464–470 (2021).

67. Chalkias, A. *et al.* Patients with colorectal cancer are characterized by increased concentration of fecal hb-hp complex, myeloperoxidase, and secretory IgA. *American Journal of Clinical Oncology* **34**, 561–566 (2011).

68. Pleguezuelos-Manzano, C. *et al.* Mutational signature in colorectal cancer caused by genotoxic pks+E. coli. *Nature* **580**, 269–273 (2020).

69. Reikvam, D. H., Derrien, M. & Islam, R. Epithelial-microbial crosstalk in polymeric Ig receptor deficient mice. *European journal of ...* (2012) doi:10.1002/eji.201242543.

70. Bharathkar, S. K. *et al.* The structures of secretory and dimeric immunoglobulin A. *Elife* **9**, e56098 (2020).

71. Tsuruta, T. *et al.* The amount of secreted IgA may not determine the secretory IgA coating ratio of gastrointestinal bacteria. *Fems Immunol Medical Microbiol* **56**, 185–189 (2009).

72. Burrows, P. D. & Cooper, M. D. IgA Deficiency. *Advances in Immunology*.

73. Dmitrieva-Posocco, O. *et al.* β-Hydroxybutyrate suppresses colorectal cancer. *Nature* **605**, 160–165 (2022).

74. Dreyfus, C. *et al.* Highly Conserved Protective Epitopes on Influenza B Viruses. *Science* **337**, 1343–1348 (2012).

75. Miyoshi, H. & Stappenbeck, T. S. In vitro expansion and genetic modification of gastrointestinal stem cells in spheroid culture. *Nat. Protoc.* **8**, 2471–2482 (2013).

76. Domènech-Moreno, E. *et al.* Tellu: an object detector algorithm for automatic classification of intestinal organoids. *Dis. Model. Mech.* **16**, dmm049756 (2023).